Renewable Energy 116 (2018) 244–264

Contents lists available at ScienceDirect

Renewable Energy

journal homepage: www.elsevier.com/locate/renene

Performance comparison of wind turbine based doubly fed induction generator system using fault tolerant fractional and integer order controllers

Muhammad Asghar [a], Nasimullah [b, *]

[a] CECOS University Peshawar, Pakistan
[b] City University of Science and IT, Peshawar, Pakistan

ARTICLE INFO

Article history:
Received 26 August 2016
Received in revised form
17 December 2016
Accepted 4 January 2017
Available online 5 January 2017

Keywords:
Wind turbine
DFIG
Active and reactive power control
Fractional calculus
Fault tolerance

ABSTRACT

A typical grid connected wind energy system is always associated with the nonlinear dynamics, uncertainties and external disturbances. Moreover as per the adopted grid codes and in the occurrence of specific faults the wind energy system should remain connected to the grid for a defined time period. Keeping in view all the effects this article proposes a high performance fault tolerant fractional order control system for the rotor side converter of a doubly fed induction generator (DFIG). The base line controller is formulated using novel fractional order sliding manifolds and the stability of the closed loop is ensured using fractional order Lyapunov theorem. As a case study the faults are introduced in the rotor current sensors and a model based fault tolerant rotor current estimation algorithm is proposed which is based on the stator measured currents and the voltages. Numerical results are presented to show the superiority of the proposed base line fractional order control method over the classical sliding mode control system in normal operating conditions. Finally the proposed algorithm is tested under the rotor current sensors fault and the results under faulty conditions are compared to that without faults.

1. Introduction

Energy is an important factor for the prosperity of the world. However due to the rapid industrial developments modern world is facing the problems of the greenhouse gases and the toxic wastes. Moreover by a recent survey the reservoirs of the major sources of the energy such as petroleum, coal, natural gas and the byproducts are depleting out quickly. A small percentage of the total power produced around the world is based on the hydro and nuclear sources. In comparison to the hydel power the nuclear fuel is very rare and it poses severe threats to the environment. So for all these reasons the future energy needs of the modern world must be based on the clean, cheap, readily available and environment friendly sources i.e. renewable energy.

Wind turbines utilize the kinetic energy of the wind and it is one of the cleanest natural energy source. Doubly fed induction generator (DFIG) is an important component of the variable speed wind farms system. DFIG offers many advantages, such as operation under variable speed, torque control, low inverter cost and flexibility for active and reactive direct power control [1]. The stator of the DFIG is usually directly connected to the three phase grid while the connectivity of the rotor side is done via back to back converters [2].

The variable speed wind energy system is preferred over fixed speed due to many reasons. Among these are lesser stresses on the mechanical structure, active and reactive direct power control and the reduction in acoustic noise [3]. Manufacturers are striving to develop larger wind turbines in the range of 3–6 MW. These large wind turbines find applications in the variable speed operation. Variable speed operation can be achieved by pitch angle control using a directly coupled synchronous generator (without gear box) or a doubly fed induction generator (DFIG).

In the presence of the nonlinear phenomena's the control of rotor and grid side converters is a challenging task. The stator's active and reactive powers are directly controlled through the rotor side converter. Several control techniques have been proposed for the rotor side converter in the past with promising results. Vector control using proportional integral (PI) method is a broadly used technique for the control of DFIG based wind turbine systems [4–6]. However there are many challenges involved in the optimal

* Corresponding author.
E-mail address: nasimullah@cusit.edu.pk (Nasimullah).

http://dx.doi.org/10.1016/j.renene.2017.01.008
0960-1481/

design of the PI controllers. For example many nonlinear effects such as un-modeled dynamics, unknown disturbances and parameter variations may cause the closed loop system's response to deviate from its desired value. A model predictive controller is proposed by the authors of [7]. The proposed MPC controller showed promising results against system uncertainties and unmodelled dynamics. Some limitations of MPC include the high computational cost, accuracy in process modeling and the lack of optimal performance over the entire horizon. The authors of [8] proposed a robust state feedback control method for the rotor and grid side converters of a DFIG. In comparison to the classical control methods the robust state feedback control ensured the effective cancellation of the disturbances with faster convergence property. In Ref. [9] a robust H_∞ control strategy is investigated to improve the active power control loop's performance of the rotor side converter. Simulation results demonstrated that the H_∞ controller is robust to system's uncertainties. Artificial intelligence (AI) methods such as fuzzy and neural networks find numerous applications in the modern control theory. Both the fuzzy systems and artificial neural networks are model free schemes and have the ability to approximate the unknown nonlinearities. Thus both these techniques turns out to be a good choice for the control of nonlinear systems such as DFIG based wind farms. In Ref. [10] an artificial neural network based robust tracking control is derived and the results are compared with classical PI controller. From the comparative study it was found that neural network based controller is more robust against parameter variation. Similarly the authors of [11] proposed fuzzy logic based robust control scheme for the rotor side converter of the DFIG and the performance of the proposed scheme have been verified. From the above cited work, although the AI based control methods show promising results but there are several challenges in the design of these controller which include the selection of the rules, membership functions, type and number of neurons and hidden layers etc. Adaptive back stepping control approach is a popular choice for many researchers. In Ref. [12] an adaptive robust control approach is investigated for the rotor and grid side converters of the DFIG based wind energy system.

Variable structure control theory has been widely utilized for both linear and nonlinear systems. Classical sliding mode control (SMC) method is robust against system uncertainties with known upper bounds however the major limitations of this method include the high frequency chattering and its unsuitability from the implementation point of view [13]. The authors of [13–16] proposed classical sliding mode based active and reactive power loops for the rotor and grid side converters with asymptotic convergence of the errors. To achieve the finite time convergence, a nonlinear error surface based fast and adaptive terminal sliding mode control strategy is implemented for the active power control of the rotor side converter [17]. In order to minimize the chattering phenomena several hybrid control techniques have been proposed such as fuzzy SMC, adaptive SMC and higher order SMC [18–23]. In Refs. [18,19] fuzzy SMC based controllers are used for the rotor side converter of the DFIG based system. In Refs. [20,21] the authors proposed robust higher order sliding mode controller for the active and reactive power control. Similarly a novel adaptive higher order sliding mode control system is investigated for the converters control of doubly fed induction generator [23].

Fractional order control theory is an emerging research area which finds applications in many fields such as engineering, medical science, financial systems and biosciences [24]. The basic theory of fractional order differentiation and integrals is well explained in Refs. [25,26]. In general fractional order controllers have more degree of freedom as compared to the integer order [27]. Hence the fractional order controllers can be tuned for the optimum dynamic response, while the robustness remain intact. The stability of the fractional order systems has been discussed in details by the authors of [28]. Moreover the authors in Refs. [29–36] proposed fractional order Lyapunov theorem for the derivation of the fractional order controllers.

The above cited work is focused only on the DFIG based variable speed wind energy systems and up to the date control methods for back to back converters. As per the adopted grid codes and in the occurrence of specific faults the wind energy system should remain connected to the grid for a defined time period. In order to fulfill the above mentioned requirement the feedback control system must be fault tolerant. The active and reactive power control loops of DFIG based wind energy system require the stator and rotor current's measurements to be used as feedback signals. Failure of one or more current sensors will greatly affect the continuous and reliable operation of the wind energy system as per the adopted grid codes [37,38]. In order to detect, isolate and identify a fault, several techniques have been proposed for real time monitoring and fault diagnosis of different systems. The authors of [39–41] presented comprehensive surveys on real time fault diagnosis and fault tolerant control system methods. The fault diagnosis and tolerant methods are divided in several categories that include the detailed discussions over the model based, signal based, knowledge based and hybrid approaches. With accurate knowledge of the systems parameters the model based fault diagnosis and tolerant methods become the obvious choice due to its simplicity and easy interpretation. The model based methods utilize state observers for online monitoring and the detection of faults. The fault isolation and identification is done through the residual. In Refs. [42–47] different model based fault diagnosis and tolerant methods that include the unknown input observer based robust fault estimation, fault estimation using fuzzy descriptor, linear approaches and identified fuzzy models have been discussed. A novel signal based method for the online monitoring of the micro mill has been proposed by the authors of [48]. Based on the probabilities densities of the force wave form, the tool condition is estimated. A data driven fault diagnosis method is proposed in Ref. [49] and the fault classification is done using the probabilistic principal component analysis with hidden Markov model. In Ref. [41] a clear understanding has been developed for both the passive and active fault tolerant control methods. The active fault tolerant control methods are the most effective and the popular choices for many researchers. The authors of reference [50] has successfully implemented an active fault tolerant control method for off shore wind turbine model.

Based on above literature survey this article formulates a fault tolerant fractional order sliding mode controller for the active and reactive power control of a doubly fed induction generator based wind energy system. The derived mathematical model of the system is subject to nonlinearities, external disturbances and parameter variations. An active fault tolerant scheme is adopted to reconstruct the rotor currents. Finally the performance of proposed controller is compared with integer order sliding mode control method under normal and faulty situations. The rest of the paper is organized as following. In Section 2 basic theory of fractional calculus is discussed. In Section 3 the mathematical models of the wind turbine system and the DFIG systems are formulated. In Section 4, the proposed controllers are derived and the stability is ensured. Section 5 discusses the fault tolerant algorithm and the fault reconstruction of the rotor currents. The results are discussed in Section 6. Finally the conclusion is made.

2. Basic definitions for fractional calculus

Fundamental fractional operator is represented as ${}_aDt\alpha$ [30].

$$ {}_aD_t^{\alpha} \cong D^{\alpha} = \begin{cases} \dfrac{d^{\alpha}}{dt^{\alpha}} & ,R(\alpha) > 0 \\ 1 & ,R(\alpha) = 0 \\ \int_a^t (d\tau)^{-\alpha} & ,R(\alpha) < 0 \end{cases} \tag{1} $$

Here α represents the order of the fractional operator and R (α) represents the set of real numbers. The following three definitions are used for the general fractional operator [30].

2.1. Definition 1

The αth order Riemann–Liouville fractional derivative and integration of a function $f(t)$ with respect to t is given by Ref. [29].

$$ {}_aD_t^{\alpha} f(t) = \frac{d^{\alpha}}{dt^{\alpha}} f(t) = \frac{1}{\Gamma(m-\alpha) dt^m} \int_{\alpha}^{t} \frac{f(\tau)}{(t-\tau)^{\alpha-m+1}}\, d\tau \tag{2} $$

$$ {}_aD_t^{-\alpha}\ f(t)\ = I^{\alpha} f(t) = \frac{1}{\Gamma(\alpha)} \int_{\alpha}^{t} \frac{f(\tau)}{(t-\tau)^{1-\alpha}} \mathrm{d}\tau \tag{3} $$

Here **"m"** is the first integer larger than **"a"** such as $m-1<\alpha<m$, $t-\alpha$ is the interval of integration and G is Euler's Gamma function.

2.2. Definition 2

The αth order Caputo fractional derivative expression of a continuous function is expressed as [29].

$$ {}_aD_t^{\alpha} \cong D^{\alpha} = \begin{cases} \dfrac{1}{\Gamma(n-\alpha)} \int_{\alpha}^{t} \dfrac{f^n(\tau)}{(t-\tau)^{\alpha-n+1}} \mathrm{d}\tau & (\mathrm{n}-1 \le \alpha < \mathrm{n}) \\ \dfrac{d^m}{dt^n} f(t) & (\alpha = \mathrm{n}) \end{cases} \tag{4} $$

2.3. Definition 3

The GL definition of order α is expressed as [29].

$$ {}_a^{GL}D_t^{\alpha} f(t) = \lim_{h \to 0} \frac{1}{h^{\alpha}} \sum_{j=0}^{[(t-\alpha)/h]} (-1)^j \binom{\alpha}{j} f(t-jh) \tag{5} $$

Here h represents the time step and $\Gamma(.)$ represents the Gamma function

$$ \binom{\alpha}{j} = \frac{\Gamma(\alpha+1)}{\Gamma(j+1)\Gamma(\alpha-j+1)} \tag{6} $$

2.4. Stability theorem for non-integer-order system

The stability of the non-integer systems has been discussed in the references list [28–30].

Theorem 1. *Consider the autonomous fractional differential system with caputo derivative* [28–30]:

$$ {}_0D_t^{\alpha} x(t) \big| = Ax(t),\ x(0) = x_0 \tag{7} $$

Here α is the fractional order, $x \in R^n$ and $A \in R^{n \times n}$. For the asymptotic stability of the system the following condition should hold: |Arg (spec (A)) |> $\alpha\pi/2$. With the satisfaction of the above condition the states decay towards 0 like $t^{-\alpha}$. Further the system is said to be stable if |Arg (spec (A))| $\ge \alpha\pi/2$ and |Arg (spec (A))| $= \alpha\pi/2$ have geometric multiplicity. Spec (A) denotes the eigenvalues of matrix A and Arg (.) is the argument of a complex number.

2.5. Fractional differentiator approximation

Oustaloup recursive algorithm is used to approximate the fractional operator [32].

$$ H(s) = s^{\alpha}, \alpha > 0, \tag{8} $$

The above relation can be approximated by a rational function of the form given below

$$ H(s) = K \prod_{n}^{N} = -N \frac{1 + s/\omega_{z,n}}{1 + s/\omega_{p,n}}, \alpha > 0 \tag{9} $$

Where K is the gain, 2N + 1 represent the number of poles and zeroes chosen. The parameters $\omega_{z,n}$ and $\omega_{p,n}$ are given as under

$$ \omega_{z,n} = \omega_b \left(\frac{\omega_h}{\omega_b} \right)^{\frac{n+N+\frac{1-\alpha}{2}}{2N+1}} \tag{10} $$

$$ \omega_{p,n} = \omega_b \left(\frac{\omega_h}{\omega_b} \right)^{\frac{n+N+\frac{1+\alpha}{2}}{2N+1}} \tag{11} $$

Where ω_b and ω_h are the lower and upper limits of the frequency band.

3. Wind energy conversion system model

The diagram of the DFIG based wind turbine system is shown in Fig. 1. From the block diagram it is noted that the stator side is directly connected to the grid while the rotor windings are connected to the grid via the back to back converters i.e. the rotor side converter (RSC) and the grid side converter (GSC).

3.1. Modeling of wind turbine

Wind turbine extracts energy from the wind and converts it to the mechanical energy. As a result torque is produced and the DFIG rotates. The power input from the wind is written as [33].

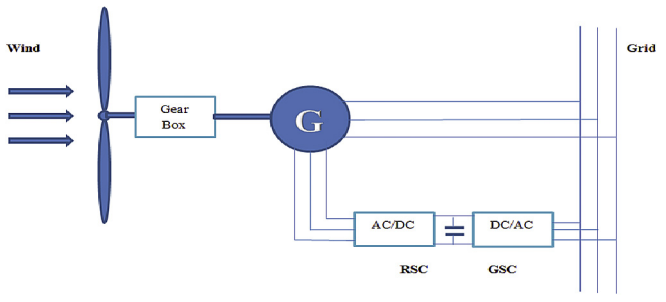

Fig. 1. Schematic of DFIG based wind turbine system.

$$P = \frac{1}{2}\rho A v^3 \tag{12}$$

The output mechanical power from the wind turbine is written as

$$P = \frac{1}{2}C_p A v^3 \tag{13}$$

The expression for the total aerodynamic power extracted from the wind can be obtained by combining Eqs. (12) and (13) as following

$$P_t = \frac{1}{2}\rho A C_p v^3 \tag{14}$$

Where ρ is the air density in kg/m^3 , A is the area of turbine blades in m^2, C_p is the power coefficient that depends on shape and geometry of turbine blades. C_p is a nonlinear function of the pitch angle β and tip speed ratio λ. The tip speed ratio is defined as

$$\lambda = \frac{\Omega_t R}{v} \tag{15}$$

Here Ω_t represents the mechanical angular shaft speed of the wind turbine in $rad/\sec$ and R is radius of the rotor of the turbine in meters. A typical mathematical relationship between C_p and λ is given in Ref. [33].

$$C_p = c_1\left(\frac{c_2}{\lambda} - 1\right)e^{\frac{-c_3}{\lambda}} \tag{16}$$

In Eq. (16) c_1,c_2 and c_3 are constants. By utilizing the power coefficient C_p only 59% of wind kinetic energy can be converted to mechanical energy [34]. For a particular speed the output power of the wind turbine will remain maximum. The tip speed ratio corresponds to the maximum speed and is represented as λ_{opt} . When $\lambda = \lambda_{opt}$ the power coefficient value is maximum ($C_p = C_{p-\max}$) and maximum power can be extracted from the wind. Typical $C_p - \lambda$ relation is shown in Fig. 2.

The Torque of wind turbine is given by

$$T_r = \frac{T_t}{G}\Omega_t = \frac{\Omega_r}{G} \tag{17}$$

Where T_r and T_t represent the generator torque and aerodynamic torque respectively, G is the gear ratio and Ω_r is generator speed. By combining Eqs. (14)–(17) the rotor reference speed and grid reference powers are calculated as

$$\Omega_{r-ref} = \frac{\lambda_{opt} G}{R} v \tag{18}$$

$$P_{grid-ref} = \frac{1}{2}\eta\rho\pi^2 C_{p-\max} v^3 \tag{19}$$

Here η is the wind turbine efficiency.

3.2. Modeling of generator

In three phase the representation of an asynchronous machine is difficult because the system dynamics are coupled and highly nonlinear. For controller formulations the d-q frame representation of a 3 phase system is more convenient. Equations describing the DFIG model in synchronous (d-q) frame are given below [35].

$$\begin{cases} V_{ds} = R_s I_{ds} + \frac{d}{dt}\varphi_{ds} - \omega_s \varphi_{qs} \\ V_{qs} = R_s I_{qs} + \frac{d}{dt}\varphi_{qs} + \omega_s \varphi_{ds} \\ V_{dr} = R_r I_{ds} + \frac{d}{dt}\varphi_{dr} - (\omega_s - \omega_r)\varphi_{qr} \\ V_{qr} = R_r I_{qs} + \frac{d}{dt}\varphi_{qr} + (\omega_s - \omega_r)\varphi_{dr} \end{cases} \tag{20}$$

Here

$$\begin{cases} \varphi_{ds} = L_s I_{ds} + M I_{dr} \\ \varphi_{qs} = L_s I_{qs} + M I_{qr} \\ \varphi_{dr} = L_r I_{dr} + M I_{ds} \\ \varphi_{qr} = L_r I_{qr} + M I_{qs} \end{cases} \tag{21}$$

$$\omega_r = P\Omega_r, \tag{22}$$

Where V_{ds}, V_{qs} denote the d-axis and q-axis stator voltage components,V_{dr} , V_{qr} are the rotor voltage components, I_{ds} , I_{qs} represent the stator current components,P represents the number of pole pairs, I_{dr} , I_{qr} are the rotor current components, R_s , R_r are the stator and rotor resistances,φ_{ds} , φ_{qs} represent the stator flux components, φ_{dr} , φ_{qr} are the rotor flux components L_s , L_r are the stator and rotor inductances, M is magnetizing inductance and ω_s , ω_r are the stator and rotor angular velocities. The mechanical dynamics of the rotating parts can be modeled as

$$J\frac{d}{dt}\Omega_r = T_{em} - T_r - f_r\Omega_r \tag{23}$$

In Eq. (23) J denotes the moment of inertia of the rotating parts, f_r is the co-efficient of friction, and T_{em} is the electromagnetic torque of DFIG. The Electromagnetic torque is a function of (d-q) components of the stator flux and rotor currents. It can written as

$$T_{em} = P\frac{M}{L_s}\left(\varphi_{qs} I_{dr} - \varphi_{ds} I_{qr}\right), \tag{24}$$

By aligning the d-axis in the direction of flux φ_s[36] we have

$$\varphi_{ds} = \varphi_s, \varphi_{qs} = 0, \tag{25}$$

Therefore by using Eqs. (24) and (25) one obtains

$$T_{em} = P\frac{M V_s}{\omega_s L_s} I_{qr} \tag{26}$$

If the per phase stator resistance is neglected with the assumption that the stator flux is also constant then the direct and quadrature voltage vectors on stator axis can be written as

$$V_{ds} = 0, V_{qs} = V_s = \omega_s \varphi_s \tag{27}$$

By using Eqs. (25) and (27) the Eqs. (20) and (21) can be simplified as

$$\begin{cases} V_{dr} = R_r I_{dr} + \sigma L_r \frac{d}{dt} I_{dr} - \sigma L_r s \omega_s I_{qr} \\ V_{qr} = R_r I_{qr} + \sigma L_r \frac{d}{dt} I_{qr} - \sigma s \omega_s I_{dr} + s\frac{M V_s}{L_s} \end{cases} \tag{28}$$

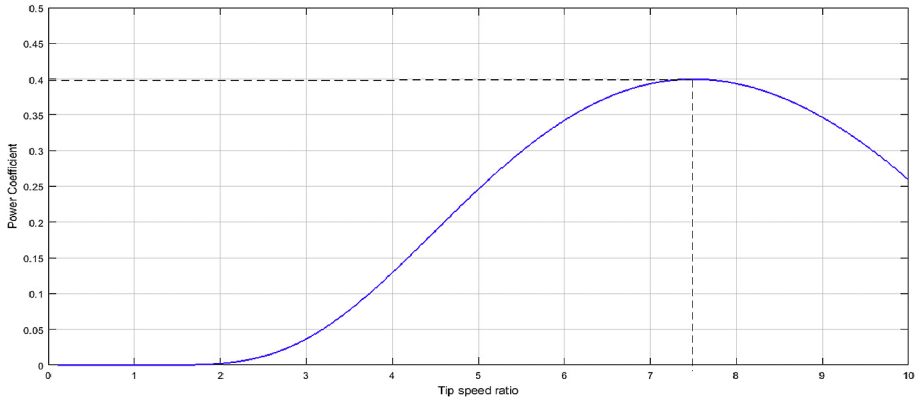

Fig. 2. Typical $C_p - \lambda$ relationship.

$$\begin{cases} P_s = -\dfrac{MV_s}{L_s} I_{qr} \\ Qs = \dfrac{V_s^2}{\omega_s L_s} - \dfrac{MV_s}{L_s} I_{dr} \end{cases} \tag{29}$$

With

$$\sigma = 1 - \frac{M}{L_r L_s}\ ,\ s = \frac{\omega_s - \omega_r}{\omega_s} \tag{30}$$

Here "s" represents the slip. The nonlinear system's model can be written in the state space form as given in Eq. 31

$$\begin{cases} \dot{x} = F(x) + Hu = f(x) + \Delta f + hu + \Delta hu, \\ \dot{x} = F(x) + Hu = f(x) + hu + d \end{cases} \tag{31}$$

In Eq. (31) the state vector is represented as$x = \begin{bmatrix} I_{dr} & I_{qr} \end{bmatrix}^T$, the control signals $u = \begin{bmatrix} V_{dr} & V_{qr} \end{bmatrix}^T f$, h are the best available approximation (nominal model) of the functions F and H, Δf and Δh represent the uncertainties in the plant and input vector, $d = \Delta f + \Delta hu = \begin{bmatrix} d_1 & d_2 \end{bmatrix}^T$ is the vector which represents the unknown lumped uncertainty in the plant model.

$$f(x) = \begin{bmatrix} -\dfrac{R_r}{\sigma L_r} I_{dr} + s\omega_s I_{qr} \\ -\dfrac{R_r}{\sigma L_r} I_{qr} - s\omega_s I_{dr} + s\dfrac{MV_s}{\sigma L_r L_s} \end{bmatrix}, \tag{32}$$

$$h = \begin{bmatrix} \dfrac{1}{\sigma L_r} & 0 \\ 0 & \dfrac{1}{\sigma L_r} \end{bmatrix}, \tag{33}$$

4. Controller formulation

Generally the system's model can be divided into two subsystems i.e. the Electrical subsystem and the mechanical subsystem. In this section, a robust chattering free fractional order sliding mode controller (FOSMC) is proposed for the rotor side converter of the DFIG. The control scheme consists of an outer speed controller and an inner loop current controller. Since the electrical subsystem (inner loop) is faster than the mechanical subsystem (outer loop), a cascaded structure is assumed for the design of the controller. The inner loop is employed to regulate the d -axis rotor current and the electromagnetic torque, while the outer loop is used for the speed trajectory tracking. Fig. 3 shows a typical wind profile to be used for the simulations and analysis [1].

4.1. Current controller

The objective of this section is to derive a controller such that the state x should track the desired trajectory x_{ref} in the presence of the uncertainties. The reference trajectory is defined as $x_{ref} = \begin{bmatrix} I_{dr-ref} & I_{qr-ref} \end{bmatrix}^T$. From Eq. (26) we have

$$I_{qr-ref} = \frac{\omega_s L_s}{PMV_s} T_{em-ref} \tag{34}$$

The active power's reference is directly proportional to I_{qr-ref} as shown in Eq. (34). In Eq. (34) T_{em-ref} is obtained from the speed controller. The reactive power reference is written as

$$Q_{s-ref} = \frac{V_s^2}{\omega_s L_s} - \frac{MV_s}{L_s} I_{dr}, \tag{35}$$

For improved power factor the reference reactive power is set to zero. i.e. $Q_{s-ref} = 0$. From Eq. (35) we have

$$I_{dr-ref} = \frac{V_s}{\omega_s M} \tag{36}$$

The tracking error is defined as

$$e_1 = x - x_{ref} = \begin{bmatrix} e_1 & e_2 \end{bmatrix}^T = \begin{bmatrix} I_{dr} - I_{dr-ref} & I_{qr} - I_{qr-ref} \end{bmatrix}^T, \tag{37}$$

The dynamics of the system in terms of e_1 can be written as

$$\dot{e}_1 = \dot{x} - \dot{x}_{ref} = f(x) + hu + d - \dot{x}_{ref} \tag{38}$$

The fractional order sliding surface vector $S = \begin{bmatrix} S_1 & S_2 \end{bmatrix}^T$ is selected as

$$S = \begin{bmatrix} S_1 \\ S_2 \end{bmatrix} = \begin{bmatrix} c_1 D^{-\alpha} e_1 + c_2 \int \dot{e}_1 \\ c_3 D^{-\alpha} e_2 + c_4 \int \dot{e}_2 \end{bmatrix} \tag{39}$$

Where c_1, c_2, c_3 and c_4 are positive parameters and α represents the order of the fractional operator i.e.$\alpha \in (0, 1)$. By applying the fractional operator D^{α} to the both sides of Eq. (39) one obtains

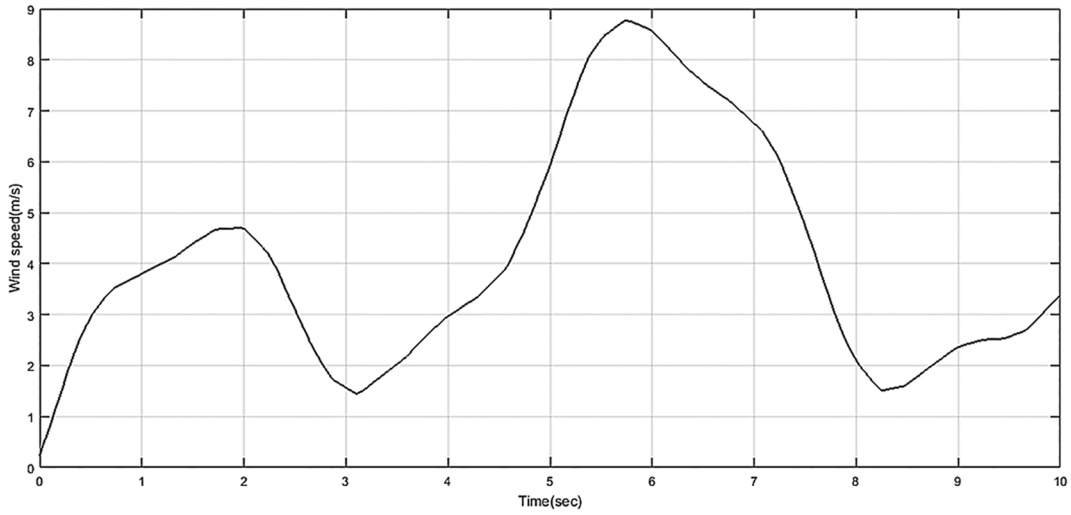

Fig. 3. Wind profile.

$$D^{\alpha}S = \begin{bmatrix} D^{\alpha}S_1 \\ D^{\alpha}S_2 \end{bmatrix} = \begin{bmatrix} c_1 e_1 + c_2 D^{\alpha-1}\dot{e}_1 \\ c_3 e_2 + c_4 D^{\alpha-1}\dot{e}_2 \end{bmatrix} \tag{40}$$

By combining Eqs. (38) and (40) one obtains

$$D^{\alpha}S = \begin{bmatrix} c_1 e_1 + c_2 D^{\alpha-1}\left(f(x) + hu + d - \dot{I}_{dr-ref}\right) \\ c_3 e_2 + c_4 D^{\alpha-1}\left(f(x) + hu + d - \dot{I}_{qr-ref}\right) \end{bmatrix} \tag{41}$$

Using Eq. (41) the proposed control law can be formulated as

$$u = u_{eq} + u_s \tag{42}$$

In Eq. (42) u_{eq} is the equivalent control which is used to compensate the nominal dynamics, while u_s is the robust term that is used to compensate the effects of the lumped uncertainty in the plant model. The equivalent controller can be obtained by setting the term$D^{\alpha}S = 0$. From Eq. (41) we have

$$u_{eq} = \begin{bmatrix} u_{eq1} \\ u_{eq2} \end{bmatrix} = \begin{bmatrix} h^{-1}\left(-f(x) + \dot{I}_{dr-ref} - \dfrac{c_1}{c_2}D^{1-\alpha}e_1\right) \\ h^{-1}\left(-f(x) + \dot{I}_{qr-ref} - \dfrac{c_3}{c_4}D^{1-\alpha}e_1\right) \end{bmatrix} \tag{43}$$

$$u_s = \begin{bmatrix} u_{s1} \\ u_{s2} \end{bmatrix} = \begin{bmatrix} h^{-1}\left(-\dfrac{k_{r1}}{c_2}D^{1-\alpha}\mathrm{sgn}\,(S_1)\right) \\ h^{-1}\left(-\dfrac{k_{r2}}{c_4}D^{1-\alpha}\mathrm{sgn}\,(S_2)\right) \end{bmatrix} \tag{44}$$

4.2. Speed controller

Speed control is derived based on the mechanical dynamics of the system. Eq. (23) can be represented as

$$\frac{d}{dt}\Omega_r = \frac{T_{em}}{J} + d_3 \tag{45}$$

$$d_3 = -\frac{T_r}{J} - \frac{f_r\Omega_r}{J} \tag{46}$$

Where T_{em} is the control input, J is best available approximate (nominal value) of the moment of inertia,d_3 is the lumped uncertainty. Speed tracking error is

$$e_3 = \Omega_r - \Omega_{r-ref} \tag{47}$$

By differentiating Eq. (47) one obtains

$$\dot{e}_3 = \dot{\Omega}_r - \dot{\Omega}_{r-ref} \tag{48}$$

By combining Eqs. (45) and (47) one obtains

$$\dot{e}_3 = \frac{T_{em}}{J} + d - \dot{\Omega}_{r-ref} \tag{49}$$

Choose a fractional order sliding surface of the form as given in Eq. 50

$$S_3 = c_5 D^{-\alpha}e_3 + c_6\int \dot{e}_3 \tag{50}$$

By applying D^{α} to Eq. 50

$$D^{\alpha}S_3 = c_5 e_3 + c_6 D^{\alpha-1}\dot{e}_3 \tag{51}$$

By putting $\dot{e}_3$ from Eq. (49) in Eq. (51), we get

$$D^{\alpha}S_3 = c_5 e_3 + c_6 D^{\alpha-1}\left(\frac{T_{em}}{J} + d - \dot{\Omega}_{r-ref}\right) \tag{52}$$

From Eq. (52), the control law can be defined as

$$\begin{cases} T_{em} = T_{em-eq} + T_{em-s} \\ T_{em-eq} = J\left(\dot{\Omega}_{r-ref} - d_3 - D^{1-\alpha}\left(\dfrac{c_5}{c_6}e_3\right)\right) \\ T_{em-s} = J\left(-\dfrac{k_{r3}}{c_6}D^{1-\alpha}(\mathrm{sgn}(s))\right) \end{cases} \tag{53}$$

Where c_5 *and* c_6 are designed parameters and k_{r3} is the discontinuous switching gain.

4.3. Stability and convergence proof

From the above analysis we know that there are two closed loops. The inner loop is formulated for the active and reactive power control and the external loop is the speed loop that sets

reference for the maximum active power to be transferred to the grid. For the stability proof only the internal loops are considered. For the external loop, the stability proof can be formulated in the same way as the internal loop. To prove the stability and the convergence proof of the inner loop, the Lyapunov function is selected as $V = \frac{1}{2}S^2$. To complete the proof the following inequality is introduced [29].

$$\left| \sum_{j=1}^{\infty} \frac{\Gamma(1+\alpha)}{\Gamma(1-j+\alpha)\Gamma(1+j)} D^j s D^{\alpha-j} s \right| \leq \lambda |s| \tag{54}$$

The parameter $\lambda = [\lambda_1\ \lambda_2]$ represent the positive constants. Applying fractional differential operator D^{α} to the Lyapunov function "V " yields [28,29].

$$D^{\alpha} V = S D^{\alpha} S + \left| \sum_{j=1}^{\infty} \frac{\Gamma(1+\alpha)}{\Gamma(1-j+\alpha)\Gamma(1+j)} D^j S D^{\alpha-j} S \right| \tag{55}$$

Using Eqs. (54) and (55), one obtains

$$D^{\alpha} V \leq S D^{\alpha} S + \lambda |S| \tag{56}$$

By combining Eqs. (41), (43), (44) and (56) one obtains

$$\begin{aligned} D^{\alpha} V &\leq S \begin{bmatrix} c_1 e_1 + c_2 D^{\alpha-1}\left(f(x) + hu + d - \dot{I}_{dr-ref}\right) \\ c_3 e_2 + c_4 D^{\alpha-1}\left(f(x) + hu + d - \dot{I}_{qr-ref}\right) \end{bmatrix} + \lambda |S| \\ &\leq S \begin{bmatrix} c_1 e_1 + c_2 D^{\alpha-1}(f(x) + h\left\{h^{-1}(-f(x) + \dot{I}_{dr-ref} - \frac{c_1}{c_2} D^{1-\alpha} e_1 - \frac{k_{r1}}{c_2} D^{1-\alpha} \mathrm{sgn}(S_1)\right\} + d_1 - \dot{I}_{dr-ref}\right) \\ c_3 e_2 + c_4 D^{\alpha-1}\left(f(x) + h\left\{h^{-1}\left(-f(x) + \dot{I}_{qr-ref} - \frac{c_3}{c_4} D^{1-\alpha} e_1 - \frac{k_{r2}}{c_4} D^{1-\alpha} \mathrm{sgn}(S_2)\right)\right\} + d_2 - \dot{I}_{qr-ref}\right) \end{bmatrix} + \lambda |S| \\ &\leq \begin{bmatrix} -\frac{k_{r1}}{c_2}\left|S_1\right| + d_1 \\ \frac{k_{r2}}{c_4}\left|S_2\right| + d_2 \end{bmatrix} + \lambda |S| \end{aligned} \tag{57}$$

From Eq. (57), by choosing $[k_{r1}\ k_{r2}] \geq [\lambda_1 + d_1\ \lambda_2 + d_2]$ the sliding condition is achieved. It means that $D^{\alpha} V \leq 0$ and $S = 0$. For the convergence proof of the system, the following Lemmas are referred:

Lemma 1. *If integral of the fractional derivative ${}_aD_t^{\alpha}$ of a function $f(t)$ exists then according to* [29].

$${}_aD_t^{-\alpha}({}_aD_t^{\alpha} f(t)) = f(t) - \sum_{J=1}^{K} \left[{}_aD_t^{\alpha-J} f(t)\right]_{a=t} \frac{(t-a)^{\alpha-J}}{\Gamma(\alpha-J+1)} \tag{58}$$

The interval is defined as: $K-1 \leq \alpha < K$ and Γ represents standard gamma function.

Lemma 2. *The fractional integral operator ${}_aD_t^{-\alpha}$ with $\alpha > 0$ is bounded such that* [29].

$$\left|\left|{}_aD_t^{-\alpha} f\right|\right|_P \leq K \left|\left|f\right|\right|_P;\ 1 \leq P \leq \infty;\ 1 \leq K \leq \infty \tag{59}$$

From Eq. (57) it is concluded that the reaching condition is satisfied i.e. $S = 0$. With this condition Eq. (26) can be simplified as

$$\begin{bmatrix} e_1 = -\frac{c_2}{c_1} D^{\alpha-1} \dot{e}_1 \\ e_2 = -\frac{c_4}{c_3} D^{\alpha-1} \dot{e}_2 \end{bmatrix} \tag{60}$$

By applying Lemma 1 to Eq. (60) one obtains

$$\begin{bmatrix} e_1 - \left[{}_{t_{r1}}D_t^{(\alpha-1)}\ e_1\right]_{t=t_{r1}} \frac{(t-t_{r1})^{\alpha-1}}{\Gamma(\alpha)} = -\frac{c_2}{c_1} D^{\alpha-1} \dot{e}_1 \\ e_2 - \left[{}_{t_{r2}}D_t^{(\alpha-1)}\ e_2\right]_{t=t_{r2}} \frac{(t-t_{r2})^{\alpha-1}}{\Gamma(\alpha)} = -\frac{c_4}{c_3} D^{\alpha-1} \dot{e}_2 \end{bmatrix} \tag{61}$$

From Eq. (61), when $t = t_{r1},\ t = t_{r2}$ the terms under fractional integral are equal to zero. i.e. $[{}_{t_{r1}}D_t^{(\alpha-1)}\ e_1]_{t=t_{r1}} \frac{(t-t_{r1})^{\alpha-1}}{\Gamma(\alpha)} = 0$, $[{}_{t_{r2}}D_t^{(\alpha-1)}\ e_2]_{t=t_{r2}} \frac{(t-t_{r2})^{\alpha-1}}{\Gamma(\alpha)} = 0$. The remaining expressions of Eq. (61) can be written as

$$\begin{bmatrix} e_1 = -\frac{c_2}{c_1} D^{\alpha-1} \dot{e}_1 \\ e_2 = -\frac{c_4}{c_3} D^{\alpha-1} \dot{e}_2 \end{bmatrix} \tag{62}$$

A more suitable form of Eq. (62) is expressed as

$$\begin{bmatrix} D^{-2} D^2 e_1 = -\frac{c_2}{c_1} D^{\alpha-1} \dot{e}_1 \\ D^{-2} D^2 e_2 = -\frac{c_4}{c_3} D^{\alpha-1} \dot{e}_2 \end{bmatrix} \tag{63}$$

Using Lemma 1, Eq. (63) is simplified and can be expressed as

$$\begin{bmatrix} e_1(t) - \left[{}_{t_{r1}}D_t^{(2-1)}\, e_1(t)\right]_{t=t_{r1}} \dfrac{(t-t_{r1})^{2-1}}{2} - e_1(t_{r1}) = -\dfrac{c_2}{c_1}D^{\alpha-1}\dot{e}_1 \\ e_2(t) - \left[{}_{t_{r2}}D_t^{(2-1)}\, e_2(t)\right]_{t=t_{r2}} \dfrac{(t-t_{r2})^{2-1}}{2} - e_2(t_{r2}) = -\dfrac{c_4}{c_3}D^{\alpha-1}\dot{e}_2 \end{bmatrix} \tag{64}$$

Using Lemma 2 the right hand side of Eq. (64) yields

$$\begin{bmatrix} -\dfrac{c_2}{c_1}D^{\alpha-1}\dot{e}_1 \le -\dfrac{c_2}{c_1}K_1\left\|\dot{e}_1\right\| \\ -\dfrac{c_4}{c_3}D^{\alpha-1}\dot{e}_2 \le -\dfrac{c_4}{c_3}K_2\left\|\dot{e}_2\right\| \end{bmatrix} \tag{65}$$

From Eqs. (64) and (65) one obtains

$$\begin{bmatrix} e_1(t) - \left[{}_{t_{r1}}D_t^{(2-1)}\, e_1(t)\right]_{t=t_{r1}} \dfrac{(t-t_{r1})^{2-1}}{2} - e_1(t_{r1}) = -\dfrac{c_2}{c_1}K_1\left\|\dot{e}_1\right\| \\ e_2(t) - \left[{}_{t_{r2}}D_t^{(2-1)}e_2(t)\right]_{t=t_{r2}} \dfrac{(t-t_{r2})^{2-1}}{2} - e_2(t_{r2}) = -\dfrac{c_4}{c_3}K_2\left\|\dot{e}_2\right\| \end{bmatrix} \tag{66}$$

When $S(t=t_{s1}\, t=t_{s2})=0$ and$[e_1(t)\, e_2(t)]=0$, then the necessary conditions of convergence are: $t_{r1}\le t_{s1}<\infty$, $t_{r2}\le t_{s2}<\infty$. Using this analysis the Eq. (66) can be expressed as

$$\begin{bmatrix} \dot{e}_1(t_{r1}-t_{s1}) \le -2e_1(t_{r1}) \\ \dot{e}_2(t_{r2}-t_{s2}) \le -2e_2(t_{r2}) \end{bmatrix} \tag{67}$$

From Eq. (67), one obtains

$$\begin{bmatrix} t_{r1} \le\ t_{s1} - \dfrac{2\|e_1(t_r)\|}{\left\|[\dot{e}_1(t)]_{t=t_r}\right\|} \\ t_{r2} \le\ t_{s2} - \dfrac{2\|e_2(t_r)\|}{\left\|[\dot{e}_2(t)]_{t=t_r}\right\|} \end{bmatrix} \tag{68}$$

From Eq. (48) it is clear that the error will converge to the equilibrium points in finite time.

5. Fault diagnosis and reconstruction of rotor current sensors measurements

The controller derived in Eqs. (43) and (44) requires the d-q components of the measured rotor currents. For reliable operation of the proposed control scheme, the measured feedback signals should be readily available even in case of the faults.

5.1. Algebraic state observer and residual generation

In this section a robust algebraic state estimator is derived for the estimation of rotor currents in d-q reference frame [51]. It is assumed that the nominal parameters of the system model are known and any uncertainty is modeled as constant disturbance. Re arranging Eq. (28) yields

$$\begin{cases} \dfrac{d}{dt}I_{dr} = -\dfrac{R_r}{\sigma L_r}I_{dr} + s\omega_s I_{qr} + \dfrac{V_{dr}}{\sigma L_r} \\ \dfrac{d}{dt}I_{qr} = -\dfrac{R_r}{\sigma L_r}I_{qr} + \dfrac{s\omega_s}{L_r}I_{dr} - \dfrac{sMV_s}{\sigma L_r L_s} + \dfrac{V_{qr}}{\sigma L_r} \end{cases} \tag{69}$$

Eq. (69) can be expressed as

$$\dot{I} = A_n I + B_n V + D_n V_s \tag{70}$$

From Eq. (70), the state vector I, control input V and the matrices are defined as

$$I = \begin{pmatrix} I_{dr} \\ I_{qr} \end{pmatrix},\ V = \begin{pmatrix} V_{dr} \\ V_{qr} \end{pmatrix},\ A_n = \begin{pmatrix} -\dfrac{R_r}{\sigma L_r} & s\omega_s \\ \dfrac{s\omega_s}{L_r} & -\dfrac{R_r}{\sigma L_r} \end{pmatrix},\ B_n = \begin{pmatrix} \dfrac{1}{\sigma L_r} \\ \dfrac{1}{\sigma L_r} \end{pmatrix},\ D_n = \begin{pmatrix} 0 \\ -\dfrac{sM}{\sigma L_r L_s} \end{pmatrix} \tag{71}$$

Assuming constant parametric uncertainties and constant disturbances, the Eq. (70) can be expressed as

$$\dot{I} = A_n I + B_n V + D_n V_s + \chi \tag{72}$$

In Eq. (72), $\chi = \Delta A I + \Delta B V + \Delta D V_s + d$. It is further assumed that the lumped disturbance term χ is extremely slow varying such that it is close to constant. By taking the Laplace transform of Eq. (72) one obtains

$$SI(s) - I(0) = A_n I(s) + B_n V(s) + D_n V_s(s) + \frac{\chi}{S} \tag{73}$$

Multiply Eq. (73) by Laplace operator "S" yields

$$S^2 I(s) - SI(0) = A_n SI(s) + B_n SV(s) + D_n SV_s(s) + \chi \tag{74}$$

By taking second derivative of Eq. (74) with respect to the operator "S" one obtains

$$\frac{d^2}{dS^2}\left[S^2 I(s)\right] = A_n\frac{d^2}{dS^2}[SI(s)] + B_n\frac{d^2}{dS^2}[SV(s)] + D_n\frac{d^2}{dS^2}[SV_s(s)] \tag{75}$$

In Eq. (75), $\frac{d^2}{dS^2}[-SI(0)] = 0$ and$\frac{d^2}{dS^2}[\chi)] \cong 0$. So Eq. (75) is free of initial conditions and other lumped disturbances.

Expanding Eq. (75) yields

$$\begin{aligned} S^2\frac{d^2}{dS^2}I(s) + 4S\frac{d}{dS}I(s) + 2I(s) = {} & A_n\left(S\frac{d^2}{dS^2}I(s) + 2\frac{d}{dS}I(s)\right) \\ & + B_n\left(S\frac{d^2}{dS^2}V(s) + 2\frac{d}{dS}V(s)\right) \\ & + D_n\left(S\frac{d^2}{dS^2}V_s(s) + 2\frac{d}{dS}V_s(s)\right) \end{aligned} \tag{76}$$

Multiplying Eq. (76) by S^{-2}

$$\frac{d^2}{dS^2}I(s)+4S^{-1}\frac{d}{dS}I(s)+2S^{-2}I(s)=A_n\left(S^{-1}\frac{d^2}{dS^2}I(s)+2S^{-2}\frac{d}{dS}I(s)\right)+B_n\left(S^{-1}\frac{d^2}{dS^2}V(s)+2S^{-2}\frac{d}{dS}V(s)\right)+D_n\left(S^{-1}\frac{d^2}{dS^2}V_s(s)+2S^{-2}\frac{d}{dS}V_s(s)\right) \tag{77}$$

In the time domain we have

$$t^2I-4\int t\,I\,dt+2\iint I\,dt^2=A_n\left(\int t^2\,Idt-2\iint tIdt^2+B_n\left(\int t^2\,V(s)dt-2\iint tV(s)dt^2\right)+D_n\left(\int t^2\,V_s(s)dt-2\iint tV_s(s)dt^2\right)\right) \tag{78}$$

From Eq. (78), the estimated current vector is expressed as

$$\hat{I}=\frac{1}{t^2}4\int t\,I\,dt-2\frac{1}{t^2}\iint I\,dt^2+\frac{1}{t^2}\left[A_n\left(\int t^2\,Idt-2\iint tIdt^2\right)\right]+\frac{1}{t^2}\left[B_n\left(\int t^2\,V(s)dt-2\iint tV(s)dt^2\right)\right]+\frac{1}{t^2}\left[D_n\left(\int t^2\,V_s(s)dt-2\iint tV_s(s)dt^2\right)\right] \tag{79}$$

Now the residual is generated as

$$R=\left|I-\hat{I}\right| \tag{80}$$

In Eq. (80) the measured rotor current in d-q frame is $I=\begin{bmatrix}I_{dr}\\ I_{qr}\end{bmatrix}$, the estimated is $\hat{I}=\begin{bmatrix}\hat{I}_{dr}\\ \hat{I}_{qr}\end{bmatrix}$ and the residua is represented as $R=\begin{bmatrix}R_{I_{dr}}\\ R_{I_{qr}}\end{bmatrix}$.

5.2. Fault detection based on the generated residuals

In occurrence of a fault the residuals of the algebraic residual generator is changing from zero to non-zero. Now to detect that a real fault has occurred, this article use the threshold detection method for fault detection in the any of the rotor currents. For this purpose threshold vector "*T*" is defined and in case of no faults the following in equality holds

$$R<T \tag{81}$$

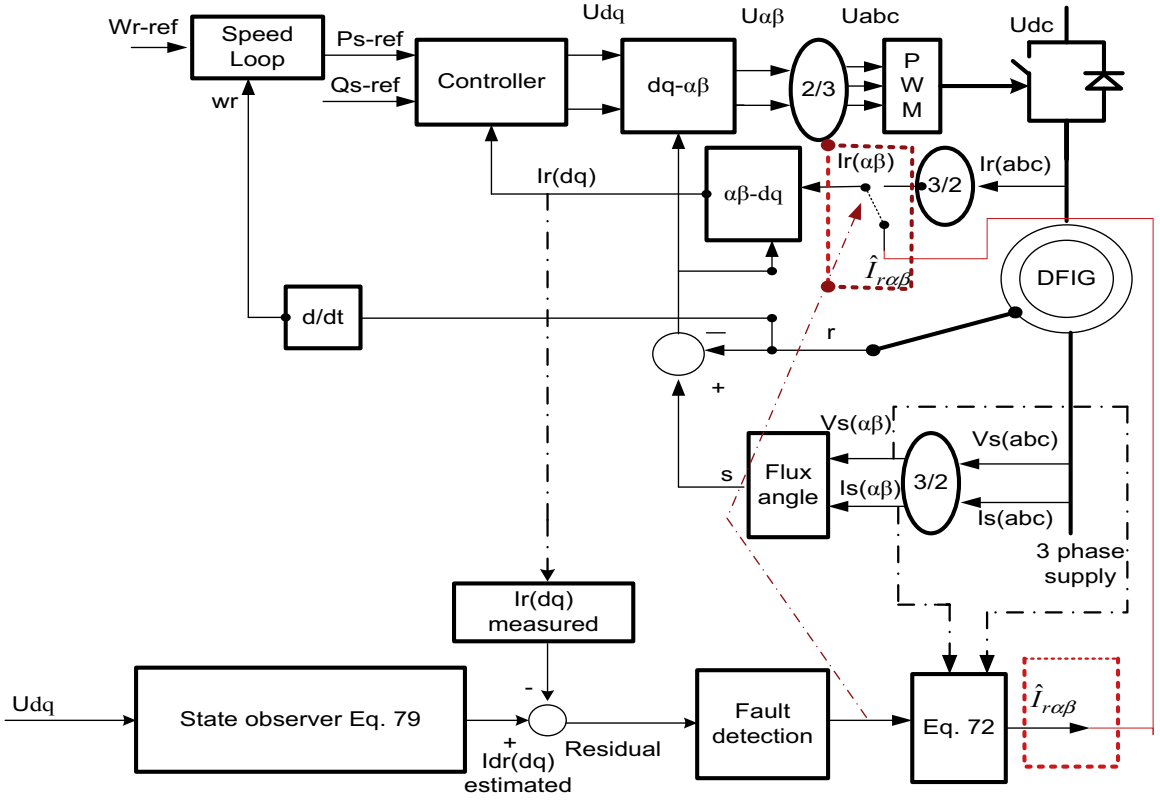

Fig. 4. Fault tolerant system for rotor current reconstruction.

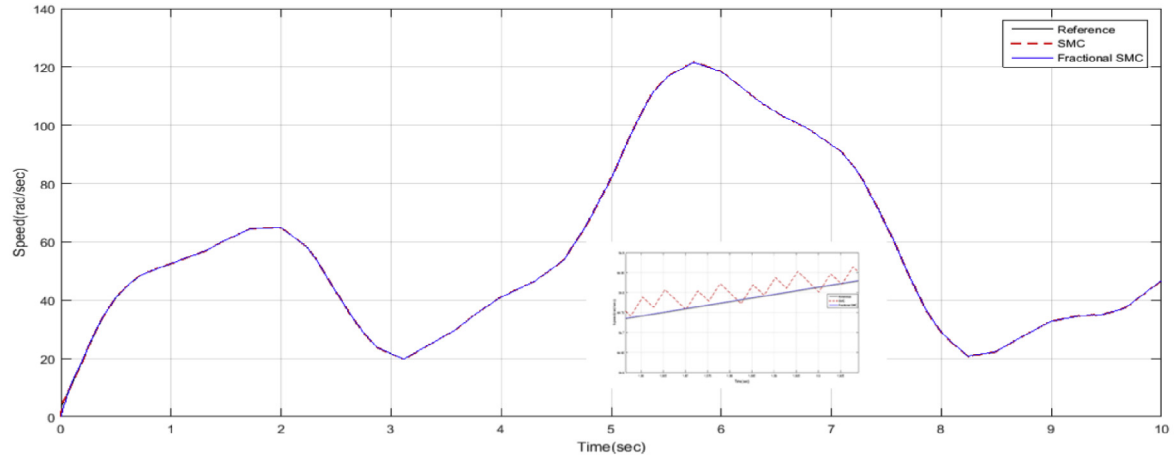

(a)

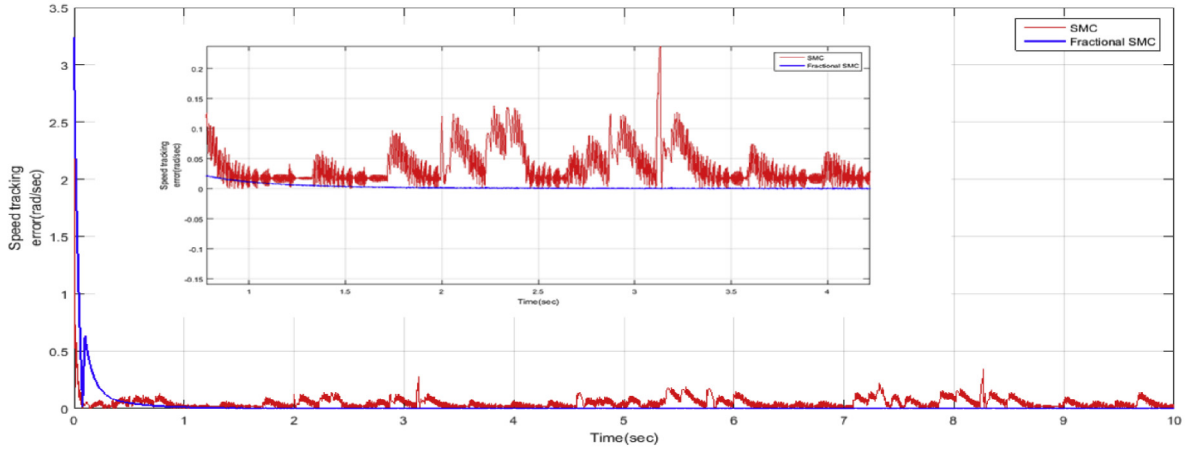

(b)

Fig. 5. (a) Rotor speed, (b) Speed tracking error.

In Eq. (81) the threshold vector is represented as $T = \begin{bmatrix} T_{Idr} \\ T_{Iqr} \end{bmatrix}$. In a situation when $R > T$, then the fault is detected. After the fault detection, the following algorithm is derived for the rotor current estimation.

5.3. Rotor current estimation based on stator measured currents and voltage

This section proposes a new algorithm to reconstruct the rotor current in case of faulty sensors. A state observer is used to estimate the rotor current dynamics in d-q frame. The residual is used to detect any fault in the rotor sensors. In case of faulty sensor the following algorithm is utilized to provide an estimation of the rotor currents.

In stator reference frame the stator flux linkage can be written as [42].

$$\begin{cases} \varphi_{s\alpha} = L_s i_{s\alpha} + L_m i_{r\alpha} \\ \varphi_{s\beta} = L_s i_{s\beta} + L_m i_{r\beta} \end{cases} \tag{82}$$

Using Eq. (82), the dynamics of rotor currents in the $\alpha - \beta$ reference is written as

$$\begin{cases} i_{r\alpha} = \dfrac{\varphi_{s\alpha} - L_s i_{s\alpha}}{L_m} \\ i_{r\beta} = \dfrac{\varphi_{s\beta} - L_s i_{s\beta}}{L_m} \end{cases} \tag{83}$$

In stator reference, the stator voltage balance equation is expressed as

$$\begin{cases} v_{s\alpha} = R_s i_{s\alpha} + \dot{\varphi}_{s\alpha} \\ v_{s\beta} = R_s i_{s\beta} + \dot{\varphi}_{s\beta} \end{cases} \tag{84}$$

By combining the first derivative of Eq. (82) and Eq. (84) one obtains

$$\begin{cases} \dot{i}_{r\alpha} = \dfrac{v_{s\alpha} - R_s i_{s\alpha} - L_s \dot{i}_{s\alpha}}{L_m} \\ \dot{i}_{r\beta} = \dfrac{v_{s\beta} - R_s i_{s\beta} - L_s \dot{i}_{s\beta}}{L_m} \end{cases} \tag{85}$$

From Eq. (85), the rotor current in $\alpha - \beta$ reference frame can be

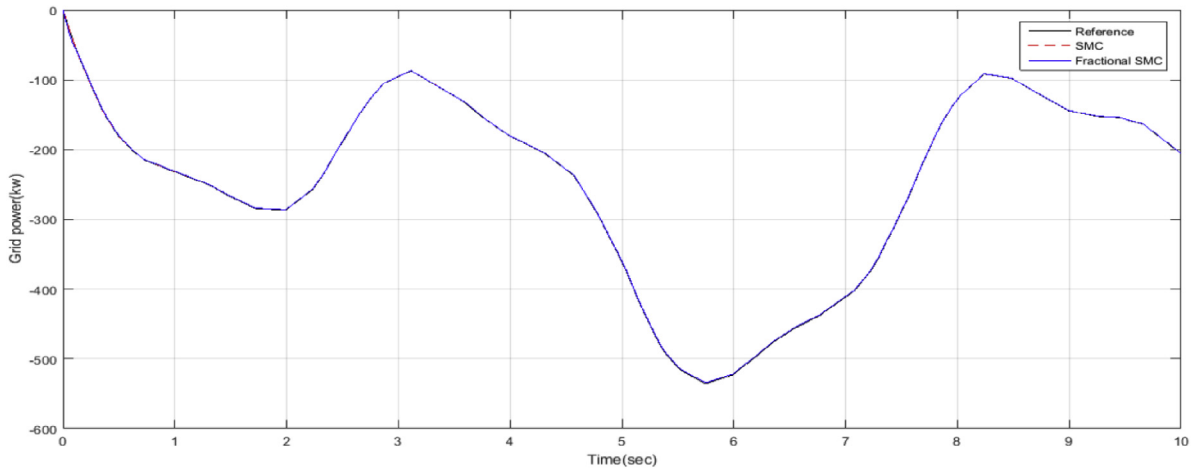

(a)

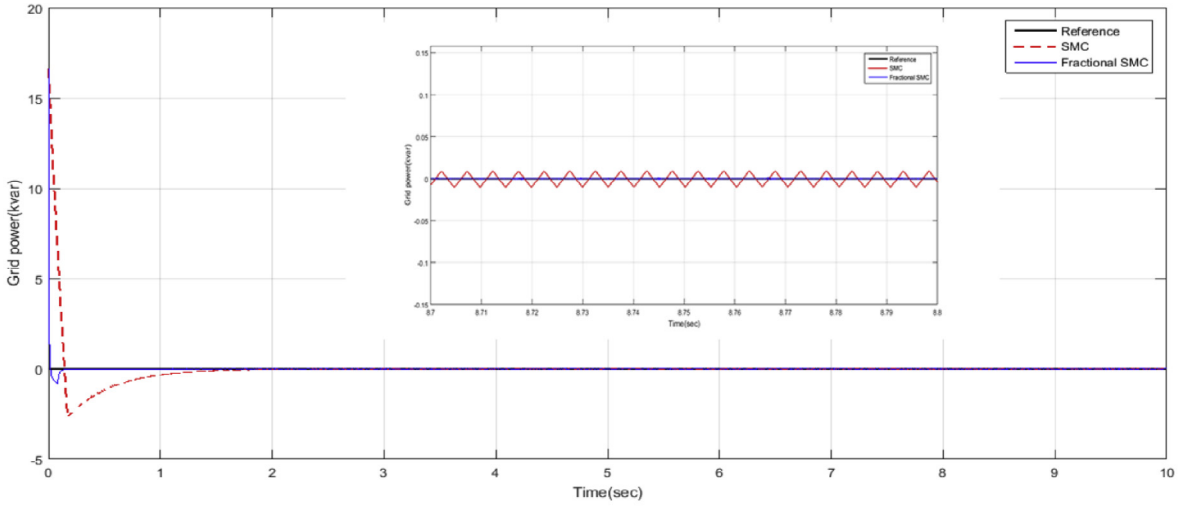

(b)

Fig. 6. (a) Active power, (b) Reactive power.

represented as

$$\begin{cases} \widehat{i}_{r\alpha} = \dfrac{\int v_{s\alpha} - R_s \int i_{s\alpha} - L_s i_{s\alpha}}{L_m} \\ \widehat{i}_{r\beta} = \dfrac{\int v_{s\beta} - R_s \int i_{s\beta} - L_s i_{s\beta}}{L_m} \end{cases} \tag{86}$$

From Eq. (86), it is obvious that the approximation of the rotor currents totally depends on the stator currents and the voltage measurements. The terms $\widehat{i}_{r\alpha}$ and $\widehat{i}_{r\beta}$ represents the approximated value of the rotor currents. Since the control equations have been formulated in $d-q$ reference frame so the approximated rotor currents are converted to $d-q$ reference frame accordingly.

$$\widehat{i}_{rdq} = dq(Eq.\ 86) \tag{87}$$

After a fault is detected in any of the rotor sensors, then the sensors are isolated and the feedback for the control law of Eqs. (43) and (44) is provided using Eq. (87). Fig. 4 shows the details of the fault diagnosis and tolerant scheme for the rotor currents reconstruction.

6. Results and discussions

In this section numerical simulations are carried out in Matlab Simulink to demonstrate the performance of the proposed fractional order sliding mode controller for DFIG based wind energy system. For comparing the results the classical sliding mode controller is given in the Appendix B. The design parameters

c_1, c_2, c_3, c_4, c_5 *and* c_6 of the proposed control are chosen as $c_1 = 200, c_2 = 2, c_3 = 5, c_4 = 2, c_5 = 10$ *and* $c_6 = 2$. The switching gains k_{r1}, k_{r2} *and* k_{r3} are chosen as$k_{r1} = 2000, k_{r2} = 2000$ *and* $k_{r3} = 500$. The parameters of the fault tolerant algorithms are selected as $T = \begin{bmatrix} \frac{I_{dr-reference}}{2} \\ \frac{I_{qr-reference}}{2} \end{bmatrix}$. The nominal parameters of DFIG and wind turbine are listed in the Appendix B. Fig. 5 shows the wind profile used as a reference for the simulations study. When initially the tracking errors are not zero the control effort has a large initial value thus the reference speed signal is passed through a first order fractional order low pass filter of the form given in Eq. 88

$$G(s) = \frac{1}{0.1\, s^{\alpha} + 1} \tag{88}$$

The numerical results are presented for both the normal and faulty condition.

6.1. Case 1: without faulty sensors

6.1.1. Case 1a: ideal condition

In case 1a it is considered that the system is running under ideal condition without any faults, parametric uncertainty and no external disturbance. Fig. 5(a) and (b) show the rotor speed tracking performance and the speed tracking error. Under ideal condition the speed tracking performance under the proposed control scheme is more accurate. Moreover as compared to the classical SMC the control signal with the proposed scheme has less chattering.

Fig. 6(a) and (b) compare the performance of the proposed control scheme with the classical SMC for the grid active and reactive power. It is concluded that the tracking performance of the proposed controller is better as compared to the classical SMC. The proposed scheme exhibits the fastest convergence time.

Current tracking error comparisons are given in Fig. 7(a) and (b). It is noted that under the action of the proposed controller the tracking response is faster and accurate. Fig. 8 (a), (b) and (c) show

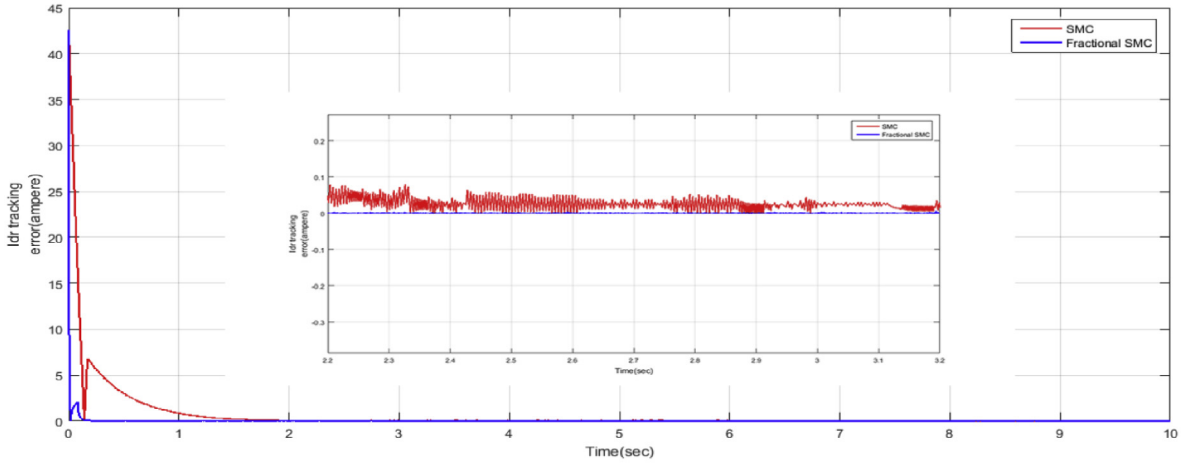

(a)

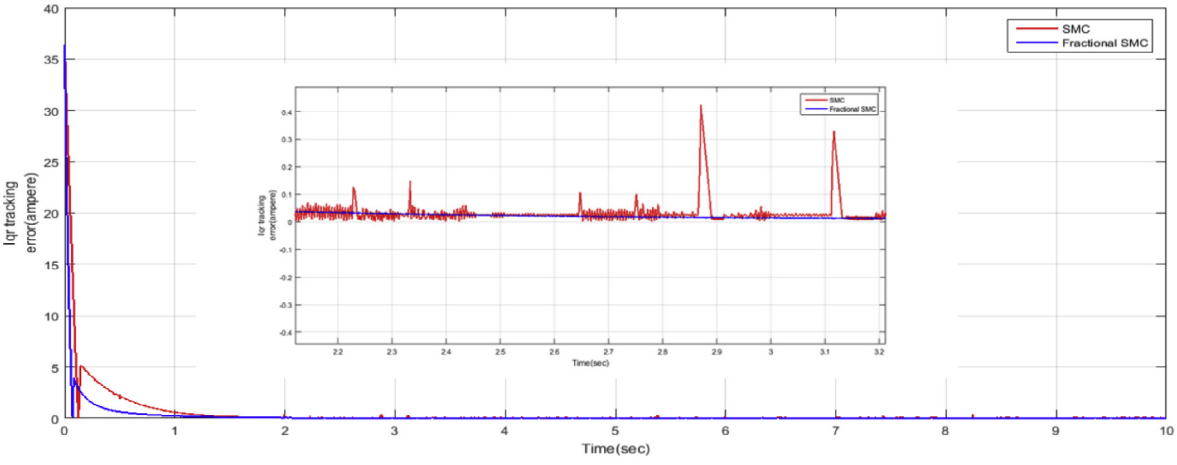

(b)

Fig. 7. (a), (b) Tracking error comparison.

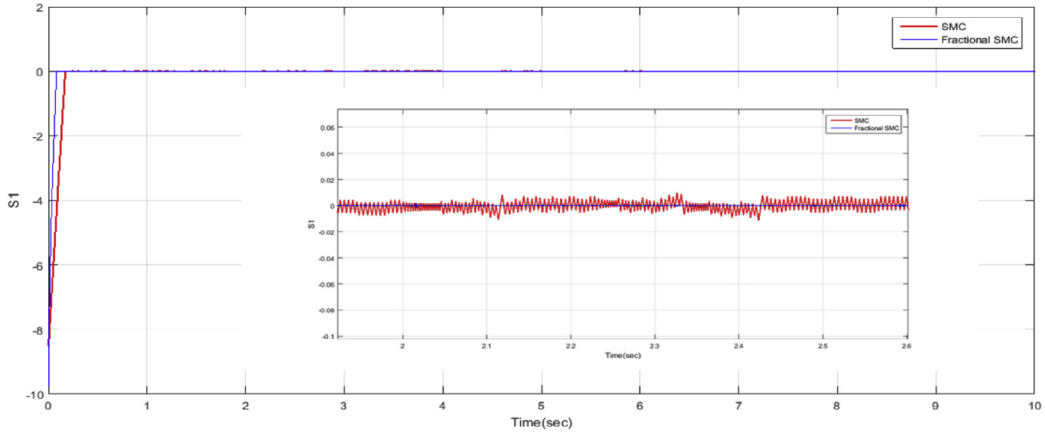

(a)

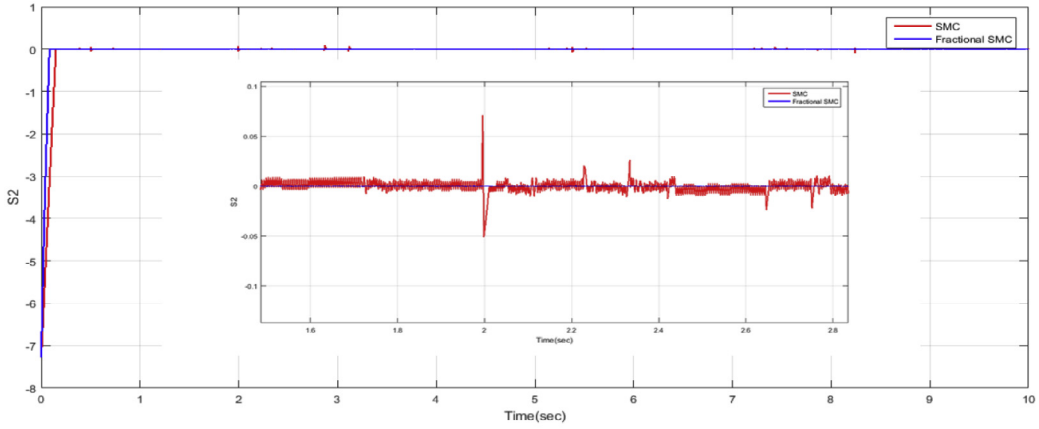

(b)

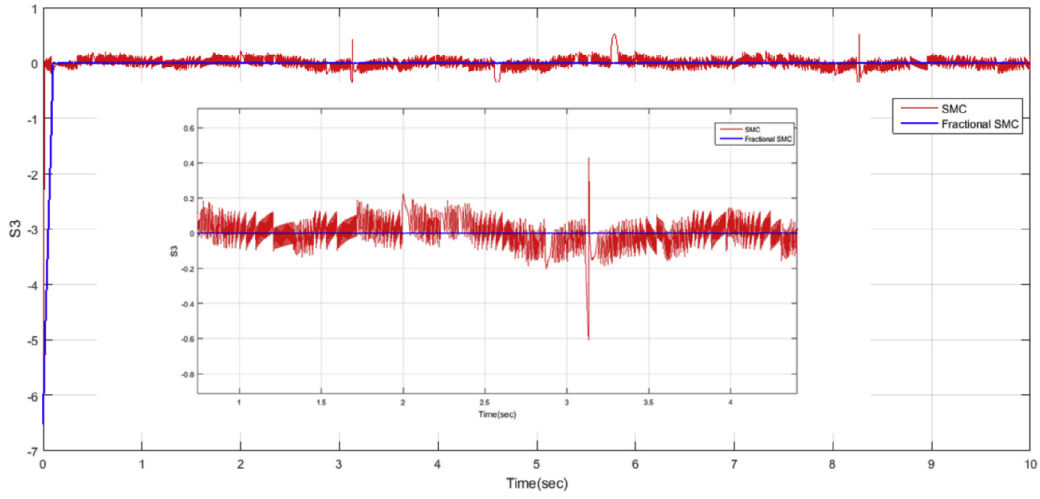

(c)

Fig. 8. (a), (b), (c) Sliding Surfaces convergence.

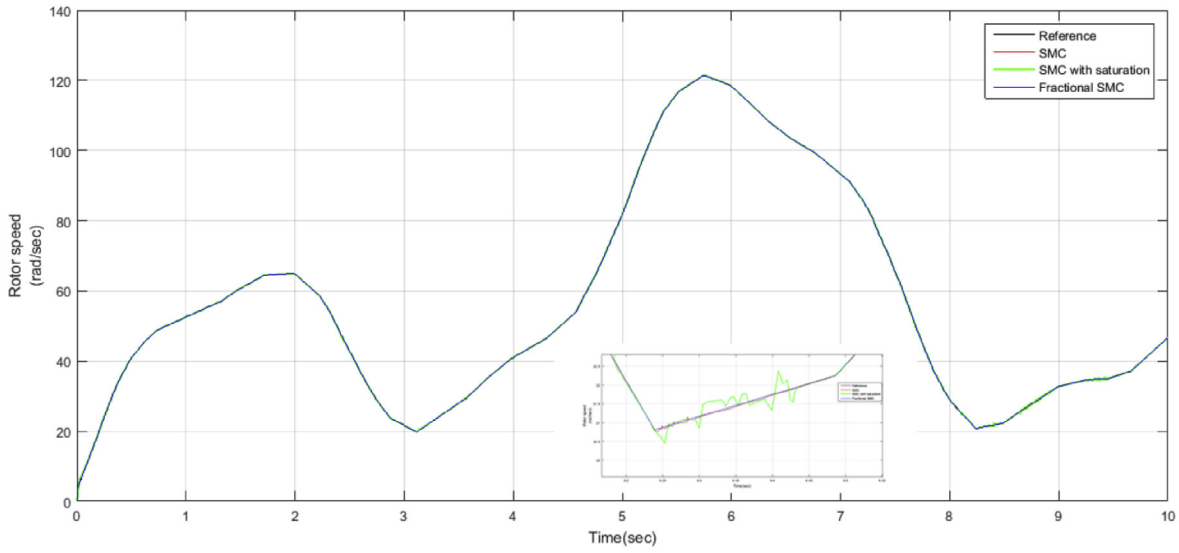

(a)

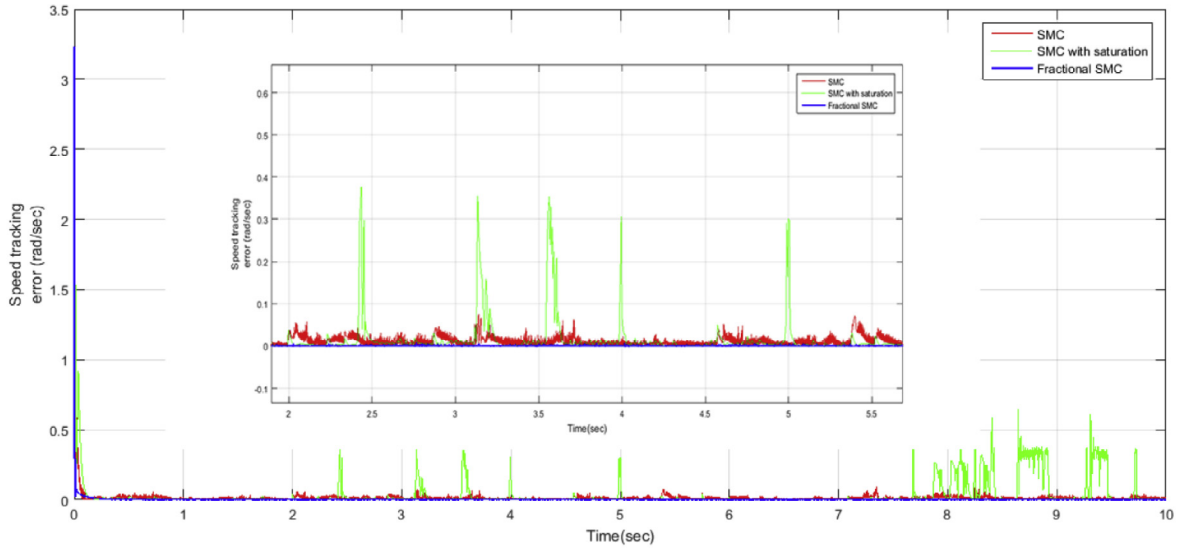

(b)

Fig. 9. (a) Rotor speed, (b) Speed tracking error.

the comparative results of the integer and non-integer sliding surfaces. From the numerical results it is confirmed that the proposed noninteger sliding surface exhibits less oscillations as compared to the classical linear surfaces. Moreover the proposed sliding surface convergences to zero in shorter time.

6.1.2. Case 1b: parametric uncertainty and external disturbances

This section presents the numerical results to illustrate the effectiveness of the proposed fractional order sliding mode controller under parametric variation and external disturbances. In Eq. (31) the lumped uncertainty term d represents the accumulative effect of parameter variations and external disturbances. It is assumed that there is 70% variation in system nominal parameters and a sinusoidal type disturbance is subject to the speed as well as the current loops. Mathematically the system dynamics including the effect of the lumped uncertainty is represented as given below.

$$\begin{cases} \dot{x} = F(x) + Hu = f(x) + hu + d \\ d = 70\%f(x) + 70\%hu + 3\sin(wt) \end{cases}$$

To avoid chattering phenomena the discontinuous *signum* function in classical SMC is replaced by *saturation* function.

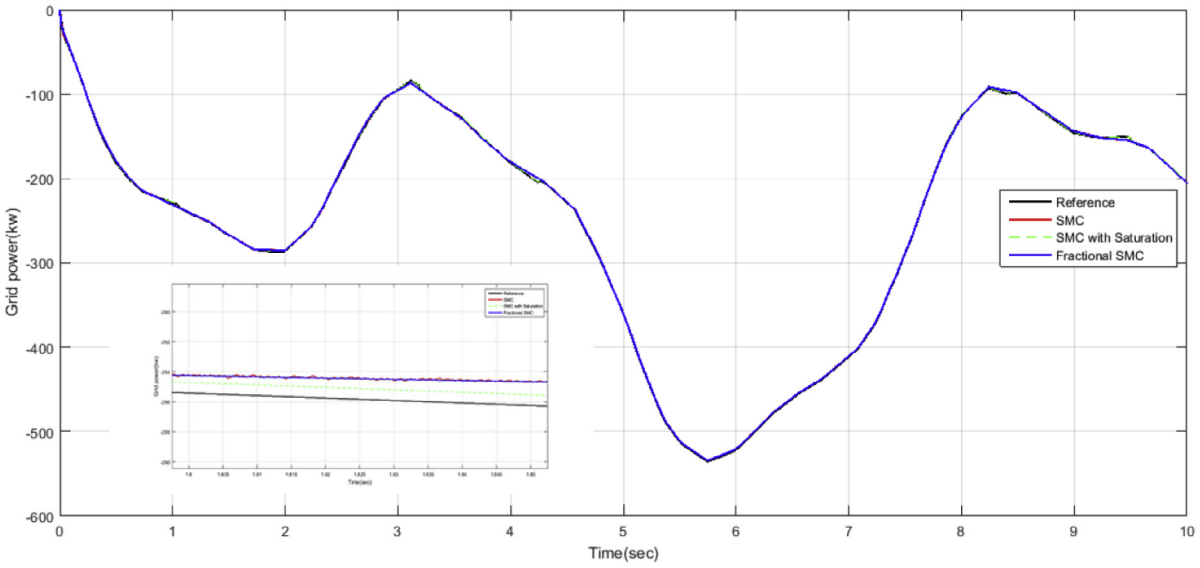

(a)

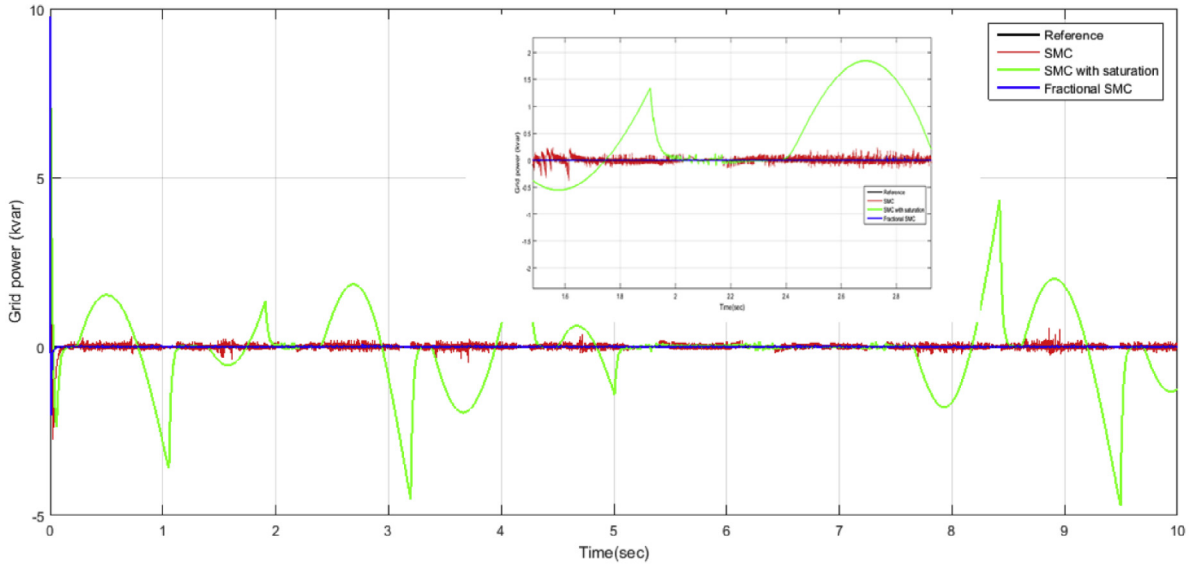

(b)

Fig. 10. (a) Active power, (b) Reactive power.

Fig. 9(a) and (b) compare the speed and error tracking performance of the wind energy system under the action of the proposed control, classical SMC and SMC with saturation function. From the numerical results it is concluded that the proposed control scheme exhibits the lowest tracking error and highest robustness against the lumped uncertainty. The active and reactive power tracking simulations are presented in Fig. 10 (a) and 10(b). From the presented numerical results it is obvious that the least tracking errors are ensured with the proposed control scheme. Although the system's performance under the classical SMC are also promising however the high frequency chattering phenomena in the control signal limits its use ability in practice. In comparison to the two methods, SMC with saturation function showed poor performance. The current tracking errors and the sliding surfaces are compared in Fig. 11(a) and (b) and 12(a) and (b). From the results presented it is concluded that the proposed controller ensures the highest robust performance, shortest convergence time and less chattering in the control signal and sliding surfaces.

6.2. Case 2: faulty rotor current sensors

In this section numerical results are presented to verify the practicality of the proposed fault tolerant rotor current estimation

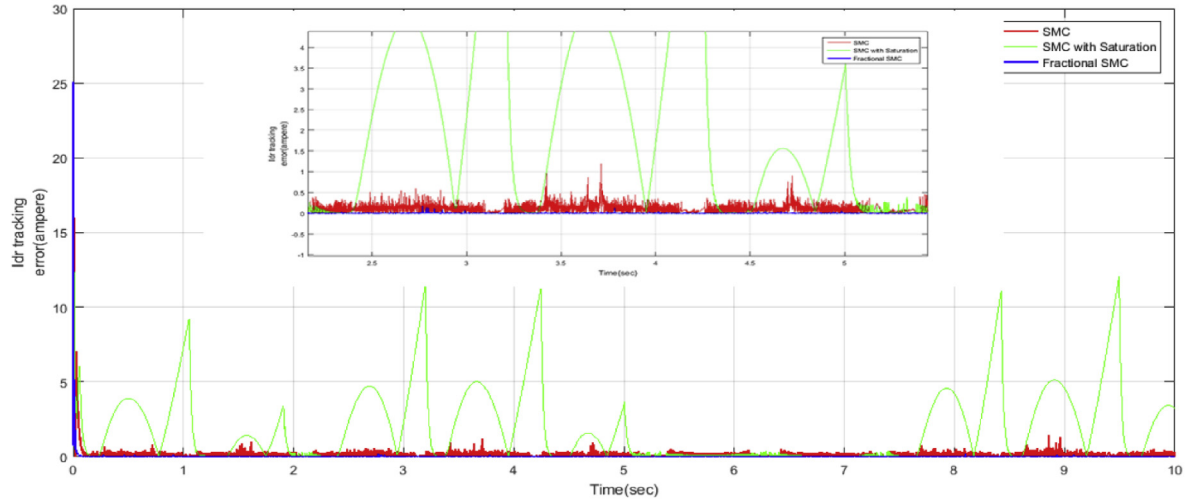

(a)

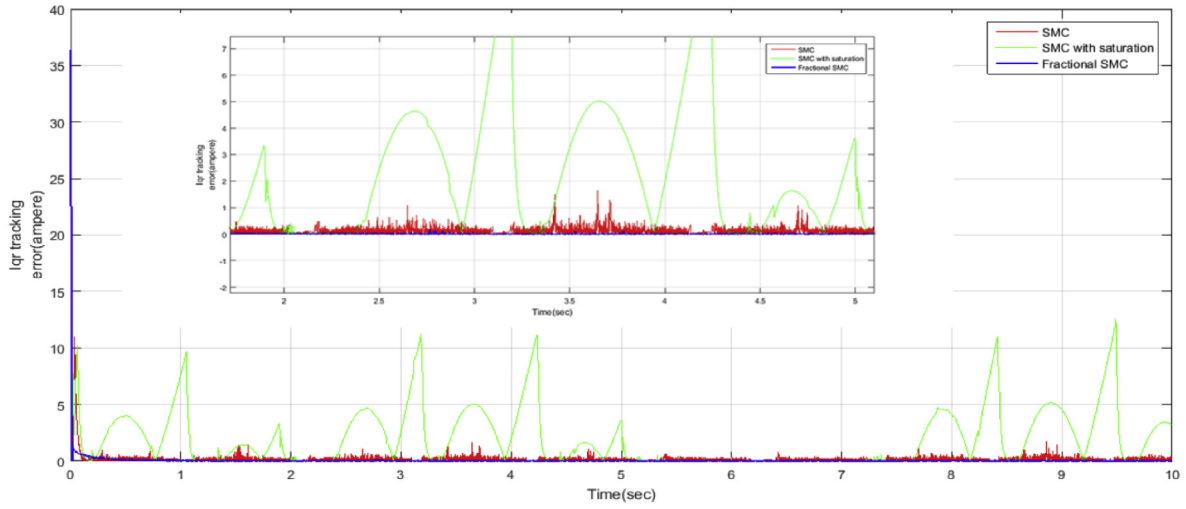

(b)

Fig. 11. (a), (b) Error tracking comparison under lumped uncertainty.

algorithm. All the rotor current sensors are assumed to be open circuit at time t = 4sec. As soon as the residual between the actual rotor currents and the observed values is greater than T then the switch is transferred to the fault reconstruction algorithm that estimates the rotor currents in alpha beta frame. Then the estimated currents are converted back to dq frame of reference which are used as feedback signals. For the sake of simplicity only the current loops are implemented. Fig. 13a shows the tracking performance of Idr under the proposed fractional order sliding mode controller. It can be seen from the results that after time t = 4sec, the estimated d component of the rotor current is practically feasible from the implementation point of view. Fig. 13(b) shows the Idr tracking error. It is confirmed from the simulation results that the current tracking error in d axis current is very small under the faulty condition. Fig. 13(c) shows the control signal Vdr simulations results. From the numerical results it is concluded that after time t = 4sec, the control signal is corrupted by fewer high frequency oscillations.

Fig. 14a, b and c show the q axis rotor current tracking performance, the tracking error and the control signal Vqr simulation results respectively. From the numerical results presented above, it is clear that the proposed fault tolerant algorithm can effectively reconstruct the rotor currents from the measured stator currents and voltages.

7. Conclusions

This article compares two version of the feedback controllers for the rotor side converter of DFIG based variable speed wind energy system. A new fault tolerant algorithm is proposed for fault detection and reconstruction of the rotor currents under faulty

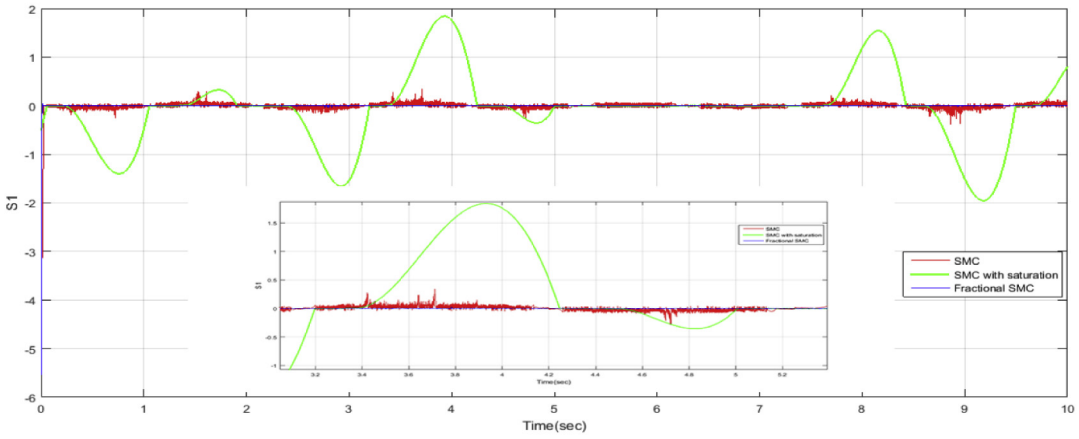

(a)

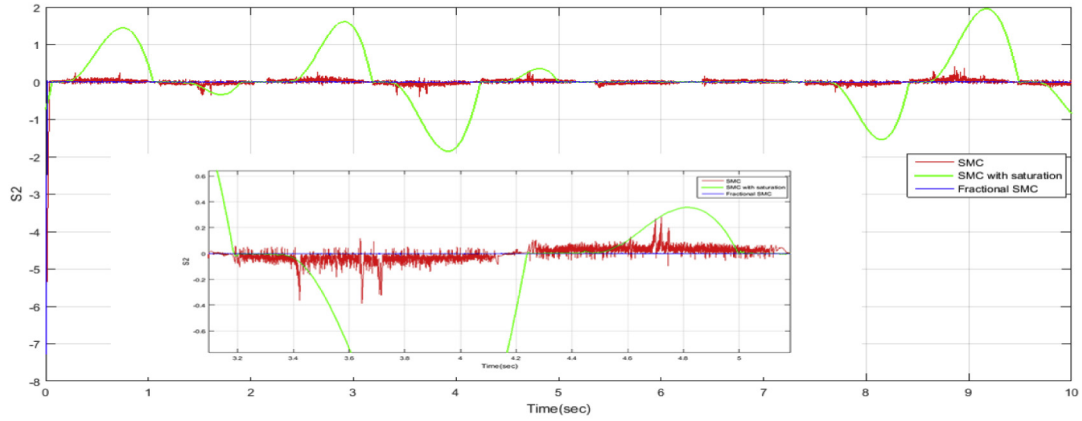

(b)

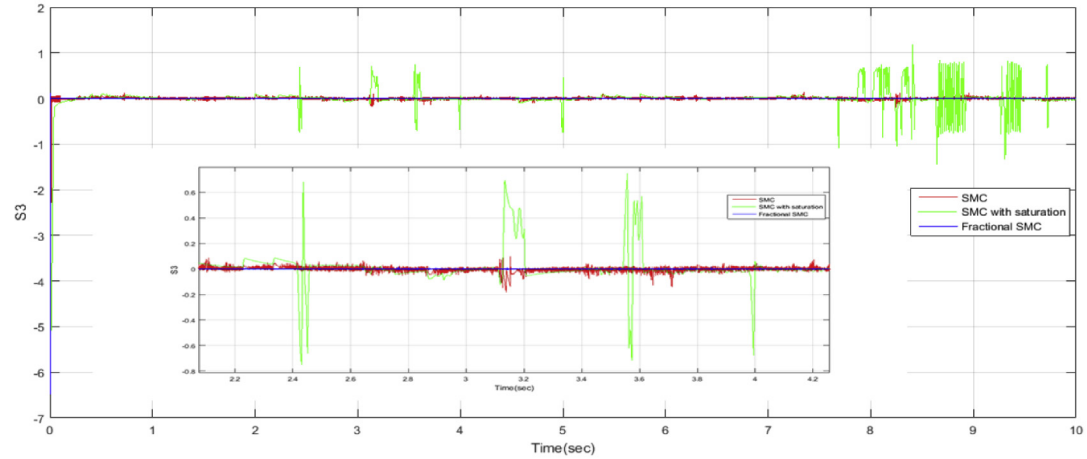

(c)

Fig. 12. (a), (b), (c) Sliding Surfaces convergence.

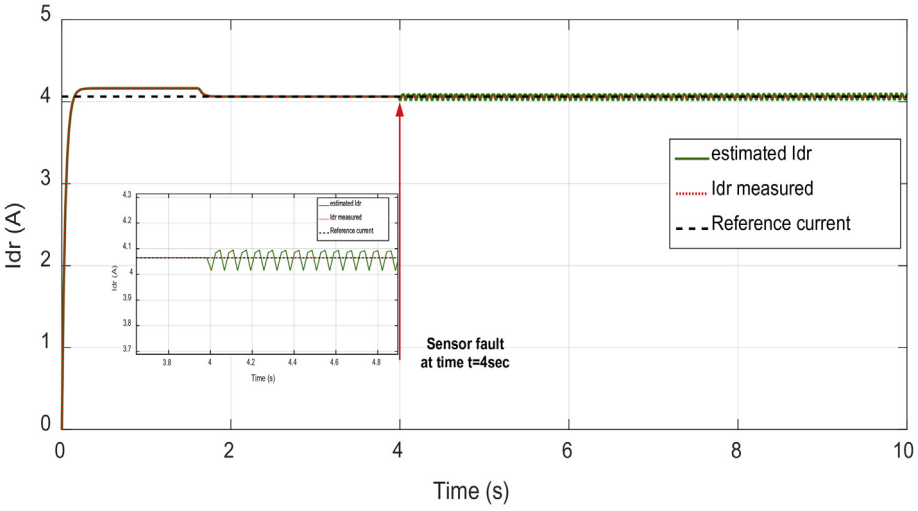

(a)

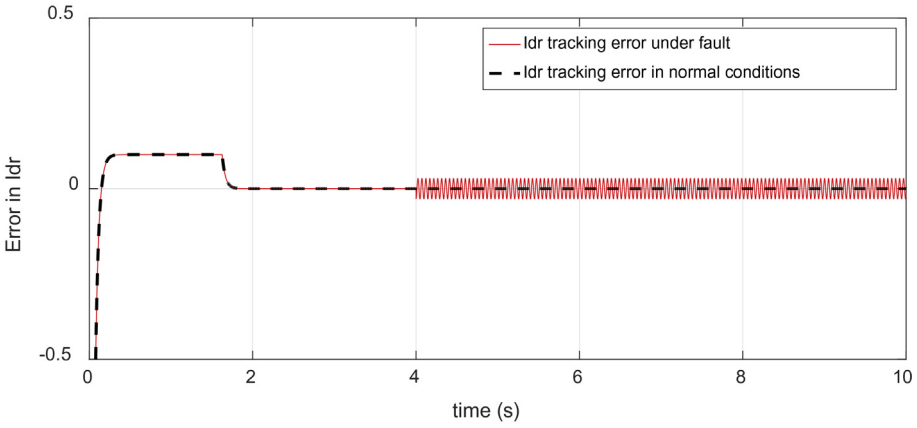

(b)

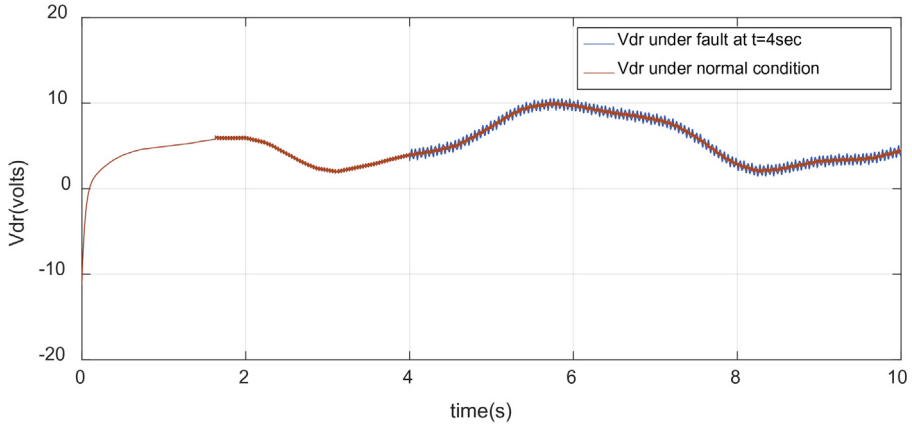

(c)

Fig. 13. Comparison under normal and rotor sensor fault (a). Idr tracking under (b) Tracking error (c) Control signal Vdr.

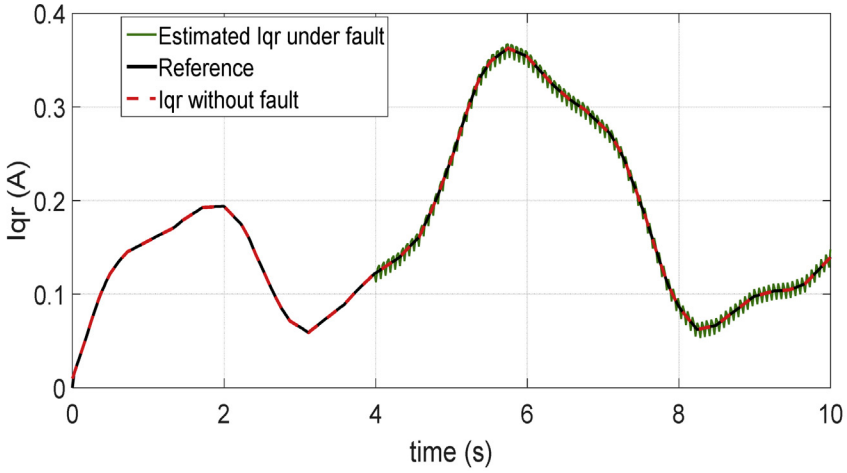

(a)

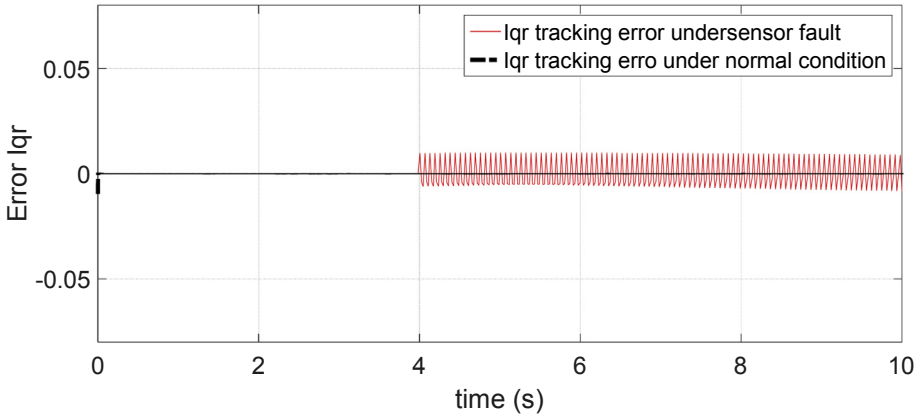

(b)

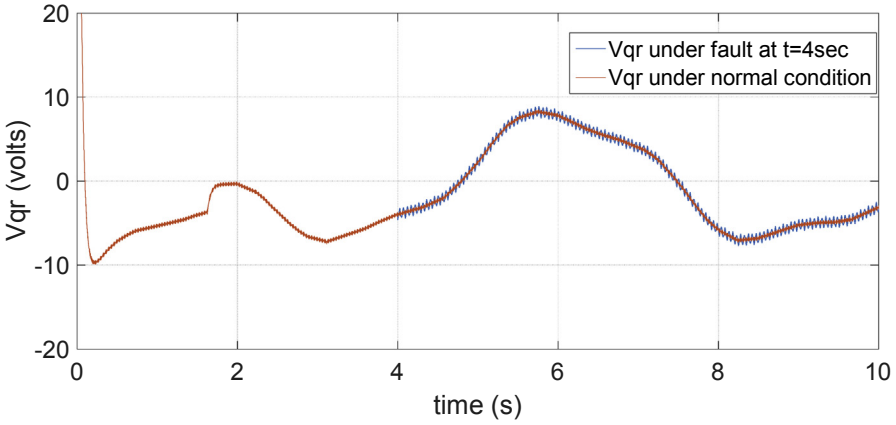

(c)

Fig. 14. Comparison under normal and rotor sensor fault (a). Iqr tracking under (b) Tracking error (c) Control signal Vqr.

conditions. The wind energy system is analyzed under the two different scenarios i.e. normal mode and faulty mode. The proposed fractional order controller is compared with integer order controllers under normal mode. From the numerical results presented it has been concluded that fractional order controller is having comparable robustness with classical sliding mode controller. Moreover the fractional order controller ensures smooth power flow and offers minimum chattering in control signal. Finally the performance of the proposed control scheme were tested with and without fault tolerant system and the from simulation results the

Table 1

DFIG	Wind turbine
Parameter value	Parameter Values
Power 660Kw	Turbine
Voltage 400V	diameter 42.33m
Frequency 50 Hz	Gear ratio 39
R_s 0.0146ΩR_r 0.0238$\Omega L_s = L_r$	c_1 9.5946
0.0306HM 0.0299	c_2 12
Hf 0.01$N\,m\,s^{-2}P$ 2	c_3 20
J 28 kg/m^2	λ_{opt} 7.5
	$C_{p-\max}$ 0.42

proposed controller turned out to be feasible for practical implementations.

Appendix A

The DFIG based wind turbine system nominal parameter values are given in Table 1.

Appendix B

Integer order sliding mode control (SMC)

Current controller derivation

Tracking error is defined in Eqs. (37) and (38). The classical sliding surface vector $S_1 = [S_1 \quad S_2]^T$ is taken as follows

$$S = \begin{bmatrix} S_1 \\ S_2 \end{bmatrix} = \begin{bmatrix} c_1 e_1 + c_2 \int e_1 \\ c_3 e_2 + c_4 \int e_2 \end{bmatrix} \tag{A1}$$

Where c_1, c_2, c_3 and c_4 are positive tuning parameters, Differentiating Eq. (A1) on both sides one can obtain

$$\dot{S} = \begin{bmatrix} \dot{S}_1 \\ \dot{S}_2 \end{bmatrix} = \begin{bmatrix} c_1 \dot{e}_1 + c_2 e_1 \\ c_3 \dot{e}_2 + c_4 e_2 \end{bmatrix} \tag{A2}$$

Using Eq. (38) and Eq. (A2) one obtains

$$\dot{S} = \begin{bmatrix} c_1 \left(f(x) + hu + d_1 - \dot{I}_{dr-ref} \right) + c_2 e_1 \\ c_3 \left(f(x) + hu + d_2 - \dot{I}_{qr-ref} \right) + c_4 e_2 \end{bmatrix} \tag{A3}$$

From Eq. (A3) the control law can be chosen as

$$u = u_{eq} + u_s \tag{A4}$$

Where u_{eq} is the equivalent control, while u_s is the robust term which is designed such that it should compensate the effects of lumped uncertainty in the plant model. The equivalent controller can be obtained by setting ($\dot{S} = 0$) in Eq. A3

$$u_{eq} = \begin{bmatrix} u_{eq1} \\ u_{eq2} \end{bmatrix} = \begin{bmatrix} h^{-1} \left(-f(x) + \dot{I}_{dr-ref} - \dfrac{c_2}{c_1} e_1 \right) \\ h^{-1} \left(-f(x) + \dot{I}_{qr-ref} - \dfrac{c_4}{c_3} e_1 \right) \end{bmatrix} \tag{A5}$$

$$u_s = \begin{bmatrix} u_{s1} \\ u_{s2} \end{bmatrix} = \begin{bmatrix} h^{-1} \left(-\dfrac{k_{r1}}{c_1} \operatorname{sgn}(S_1) \right) \\ h^{-1} \left(-\dfrac{k_{r2}}{c_3} \operatorname{sgn}(S_2) \right) \end{bmatrix} \tag{A6}$$

The reaching condition can be achieved in Eq. (6) by setting$k_{r1} > d_1$ $k_{r2} > d_2$. Moreover the signum function is defined as

$$\operatorname{sgn}(s) = \begin{cases} +1 & if \ \ s > 0 \\ 0 & if \ \ s = 0 \\ -1 & if \ \ s < 0 \end{cases} \tag{A7}$$

The Lyapunov function is

$$\left\{ \begin{matrix} V = \dfrac{1}{2} S^2 \\ \dot{V} = S\dot{S} \end{matrix} \right\} \tag{A8}$$

By combining Eq. (A3), A5, A6 and Eq. (A8) one obtains

$$\dot{V} = S\dot{S} = \begin{bmatrix} S_1 (d - \dfrac{k_{r1}}{c_1} \operatorname{sgn}(S_1)) \\ S_2 (d - \dfrac{k_{r2}}{c_3} \operatorname{sgn}(S_2)) \end{bmatrix} \leq \begin{bmatrix} S_1 |d|_{\max} - \dfrac{k_{r1}}{c_1} |S_1| \\ S_2 |d|_{\max} - \dfrac{k_{r2}}{c_3} |S_2| \end{bmatrix} \leq 0 \tag{A9}$$

Speed controller derivation

The speed tracking error is defined in Eq. (47). Classical sliding surface is given as

$$S_3 = c_5 e_3 + c_6 \int e_3 \tag{A10}$$

By taking the derivative of Eq. (A10) one can get

$$\dot{S}_3 = c_5 \dot{e}_3 + c_6 e_3 \tag{A11}$$

Putting $\dot{e}_3$ from Eq. (49) in Eq. (A11) we get

$$\dot{S}_3 = c_5 \left(\frac{T_{em}}{J} + d - \dot{\Omega}_{r-ref} \right) + c_6 e_3 \tag{A12}$$

Control law can be chosen as

$$\begin{cases} T_{em} = T_{em-eq} + T_{em-s} \\ T_{em-eq} = J \left(\dot{\Omega}_{r-ref} - d_3 - \left(\dfrac{c_6}{c_5} e_3 \right) \right) \\ T_{em-s} = J \left(- \dfrac{k_{r3}}{c_5} (\operatorname{sgn}(s_3)) \right) \end{cases} \tag{A13}$$

Where c_5 *and* c_6 are designed parameters and k_{r3} is discontinuous switching gain which is chosen greater than the lumped uncertainty. The stability of the speed controller can formulated in the similar way as explained above.

References

[1] S. Ebrahimkhani, Robust fractional order sliding mode control of doubly-fed induction generator (DFIG) based wind turbines, ISA Trans. 63 (2016) 343–354.

[2] A.A. Mohammad, Performance of control dynamics of wind turbine based on doubly fed induction generator under different modes of speed operation, in: Conference Papers in Engineering, vol. 2013, 2013, pp. 1–9.

[3] K.H. Belgacem, A. Mezouar, A. Massoum, Sliding mode control of a doubly-fed induction generator for wind energy conversion, Int. J. Energy Eng. 3 (2013) 30–36.

[4] S. Pati, S. Samantray, Decoupled control of active and reactive power in a DFIG based wind energy conversion system with conventional P-I controllers, in: IEEE International Conference on Circuit, Power and Computing Technologies (ICCPCT), 2014, pp. 898–903.

[5] Y. Bekakra, D.B. Attous, Optimal tuning of PI controller using PSO optimization for indirect power control for DFIG based wind turbine with MPPT, Int. J. Syst. Assur. Eng. Manag. 5 (2014) 219–229.

[6] R.E. Pena, R. Cardenas, J. Proboste, G. Asher, J. Clare, Sensor less control of

doubly-fed induction generators using a rotor current based MRAS observer, IEEE Transaction Industrial Electron. 55 (2008) 330–339.
[7] M.S. Lagoun, A. Benalia, M. Benbouzid, A predictive power control of doubly fed induction generator for wave energy converter in irregular waves, in: International Conference on Green Energy, 2014, pp. 26–31.
[8] F. Taveiros, L.S. Barros, F.B. Costa, Back to Back converter state feedback control of DFIG based wind Turbine, Energy 89 (2015) 896–906.
[9] H. Moradi, G. Vossoughi, Robust control of the variable speed wind turbines in the presence of uncertainties: a comparison between H∞ and PID controllers, Energy 90 (2015), 1508 – 21.
[10] Y. Djeriri, A. Meroufel, M. Allam, Artificial neural network-based robust tracking control for doubly fed induction generator used in wind energy conversion systems, J. Adv. Res. Sci. Technol. 2 (2015) 173–181.
[11] R. Ganesh, R. Senthil Kumar, K. Kaviya, Fuzzy logic controller for doubly fed induction generator based wind energy conversion system, Int. J. Innovative Res. Sci. Eng. Technol. 3 (2014) 1–9.
[12] B. Bossoufi, M. Karim, A. Lagrioui, M. Taoussi, A. Derouich, Adaptive Back-stepping control of DFIG generators for variable-speed wind turbines system, J. Electr. Syst. 10 (2014) 317–330.
[13] M.I. Martinez, G. Tapia, A. Susperregui, Sliding-mode control for DFIG rotor and grid side converters under unbalanced and harmonically distorted grid voltage, IEEE Trans. Energy Conversat. 27 (2012) 328–339.
[14] Kh Belgacem1, A. Mezouar1, A. Massoum, Sliding mode control of a doubly-fed induction generator for wind energy conversion, Int. J. Energy Eng. 3 (1) (2013) 30–36.
[15] A. Dendouga, R. Abdessemed, M. L. Bendaas and A. Chaiba, Sliding Mode Control of Active and Reactive Powers Generated by a Doubly-fed Induction Generator (DFIG), Damascus University Journal. vol. 2(24).
[16] M. Loucif, A.M. Boumediene, A. Mechernene, Nonlinear sliding mode power control of DFIG under wind speed variation and grid connection, Electroteh. Electron. Autom. 63 (2015) 23–32.
[17] R.K. Patnaik, P.K. Dash, Fast adaptive finite-time terminal sliding mode power control for the rotor side converter of the DFIG based wind energy conversion system, Sustain. Energy, Grids Netw. 1 (2015) 63–84.
[18] S.A.E.M. Ardjoun, A. Mohamed, Fuzzy sliding mode control applied to a doubly fed induction generator for wind turbines, Turk J Elec Eng Comp Sci (2015) 1–14.
[19] A. Kerboua, A. Mohamed, Hybrid fuzzy sliding mode control of a doubly-fed Induction generator in wind turbines, Rev. Roum. Des. Sci. Tech. 57 (2012) 412–421.
[20] M. Benbouzid, B. Beltran, Y. Amirat, G. Yao, J. Han, H. Mangel, Second-order sliding mode control for DFIG-based wind turbines fault ride-through capability enhancement, ISA Trans. 53 (2014) 827–833.
[21] K.D. Kerrouche, A. Mezouar, L. Boumedien, Maximized power control based on high order sliding mode for sensorless DFIG variable speed wind turbine, in: International Conference on Green Energy and Environmental Engineering, 2014, pp. 1–6.
[22] P.K. Dash, R.K. Patnaik, Adaptive second order sliding mode control of doubly fed induction generator in wind energy conversion system, J. Renew. Sustain. Energy 6 (2014) 053143.
[23] J. Bai and XC. Feng, Fractional order anisotropic diffusion for image de noising, IEEE Trans. Image Process. 16(10) 2492–2502.
[24] K. Miller, B. Ross, An Introduction to the Fractional Calculus and Fractional Differential Equations, CA: Wiley Inter science, San Francisco (, 1993.
[25] I. Podlubny, Fractional Differential Equations, New York Academic Press, 1999.
[26] M.B. Delghavi, S.S. Majidabad, A. Yazdani, Fractional-order sliding-mode control of islanded distributed energy resource systems, IEEE Trans. Sustain. Energy (2016) 1949–3029.
[27] Dennis Matignon, Stability properties for generalized fractional differential systems, ESAIM Proceedings, Fract. Differ. Syst. Models Methods Appl. 5 (1998) 145–158.
[28] M.P. Aghababa, A Lyapunov based control scheme for robust stabilization of fractional chaotic systems, Nonlinear Dyn. 78 (2014) 2129–2140.
[29] C. Li, W. Deng, Remarks on fractional derivatives, Appl. Math. Comput. 187 (2007) 777–784.
[30] F. Zhang, C. Li, Stability Analysis of Fractional Differential Systems with Order Lying in (1, 2), Advances in Difference Equations, 2011 (/2011) 213485.
[31] Z. Gao, X. Liao, Improved Oustaloup approximation of fractional-order operators using adaptive chaotic particle swarm optimization, J. Syst. Eng. Electron. 23 (2012), 145 – 53.
[32] T. Burton, N. Jenkins, D. Sharpe, E. Bossanyi, Wind Energy Handbook, second ed., Wiley, 2011.
[33] B. Kiruthiga, Implementation of first order sliding mode control of active and reactive power for DFIG based wind turbine, IJIFR Electr. Electron. Eng. 2 (2015) 2487–2497.
[34] F.K.A. Lima, E.H. Watanabe, P. Rodriguez, A.A. Luna, Simplified Model for Wind Turbine Based on Doubly Fed Induction Generator, IEEE ICEMS, Beijing (, 2011, pp. 1–6.
[35] A. Mechter, K. Kemih, M. Ghanes, Sliding mode control of a wind turbine with exponential reaching law, Acta Polytech. Hung. 12 (2015) 167–183.
[36] R. Patton, P. Frank, R. Clark, Issues of Fault Diagnosis for Dynamic Systems, Springer-Verlag, Berlin, 2000.
[37] S. Karimi, A. Gaillard, P. Poure, S. Saadate, Current sensor fault-Tolerant control for WECS with DFIG, IEEE Trans. Industrial Electron. 56 (2009) 4660–4670.
[38] A. Karthikeyan, C. Nagamani, A.B.R. Chaudhury, G.S. Ilango, Implicit position and speed estimation algorithm without the flux computation for the rotor side control of doubly fed induction motor drive, IET Electr. Power Appl. 6 (2012) 243–252.
[39] Z. Gao, C. Cecati, S.X. Ding, A survey of fault diagnosis and fault-tolerant techniques—Part I: fault diagnosis with model-based and signal-based approaches, IEEE Trans. Ind. Electron. 62 (no. 6) (Jun. 2015) 3757–3767.
[40] Z. Gao, C. Cecati, S.X. Ding, A survey of fault diagnosis and fault-tolerant techniques—Part II: fault diagnosis with knowledge-based and hybrid/active approaches, IEEE Trans. Ind. Electron. 62 (no. 6) (Jun. 2015) 3768–3774.
[41] Gao Zhiwei, Ding, X. Steven, Carlo Cecati, Real-time fault diagnosis and fault-tolerant control, IEEE Trans. Industrial Electron. 62 (6) (2015) 3752–3756. ISSN 0278-0046.
[42] Gao Zhiwei, Xiaoxu Liu, Michael Z.Q. Chen, Unknown input observer based robust fault estimation for systems corrupted by partially-decoupled disturbances, IEEE Trans. Industrial Electron. 63 (4) (2016) 2537–2547.
[43] Q. Jia, W. Chen, Y. Zhang, H. Li, Fault reconstruction and fault tolerant control via learning observers in Takagi–Sugeno fuzzy descriptor systems with time delays, IEEE Trans. Ind. Electron 62 (no. 6) (Jun. 2015) 3885–3895.
[44] T. Steffen, Control Reconfiguration of Dynamical Systems: Linear Approaches and Structural Tests, Springer Verlag, Berlin, 2005.
[45] R. Lorenz, Observers and state filters in drives and power electronics, J. Electr. Eng. 2 (2002) 19–28.
[46] S. Bennett, Model Based Methods for Sensor Fault-tolerant Control of Rail Vehicle Traction, PhD-Thesis, University of Hull, 1998.
[47] S. Simani, S. Farsoni, P. Castaldi, "Fault diagnosis of a wind turbine benchmark via identified fuzzy models, IEEE Trans. Ind. Electron. 62 (no. 6) (Jun. 2015) 3775–3782.
[48] K. Zhu, T. Mei, D. Ye, Online condition monitoring in micro-milling: a force waveform shape analysis approach, IEEE Trans. Ind. Electron. 62 (no. 6) (Jun. 2015) 3806–3813.
[49] J. Zhu, Z. Ge, Z. Song, "HMM-driven robust probabilistic principal component analyzer for dynamic process fault classification, IEEE Trans. Ind. Electron. 62 (no. 6) (Jun. 2015) 3814–3821.
[50] Fengming Shi, Ron Patton, An active fault tolerant control approach to an offshore wind turbine model, Renew. Energy 75 (2015) 788–798.
[51] G. Mamani, J. Becedas, V. Feliu-Batlle, H. Sira-Ramırez, An algebraic state estimation approach for DC motors, in: Proceedings of the World Congress on Engineering and Computer Science 2007 WCECS 2007, October 24-26, 2007 (San Francisco, USA).